



Fast radio burst dispersion measures and rotation measures and the origin of intergalactic magnetic fields

S. Hackstein,¹ M. Brüggen,¹ F. Vazza,^{1,2,3} B. M. Gaensler^{4,5} and V. Heesen¹

¹Hamburger Sternwarte, University of Hamburg, Gojenbergsweg 112, D-21029 Hamburg, Germany

²Department of Physics and Astronomy, University of Bologna, Via Gobetti 93/2, I-40129 Bologna, Italy

³Istituto di Radioastronomia, INAF, Via Gobetti 101, I-40129 Bologna, Italy

⁴Dunlap Institute for Astronomy and Astrophysics, University of Toronto, Toronto, ON M5S 3H4, Canada

⁵Department of Astronomy and Astrophysics, University of Toronto, Toronto, ON M5S 3H4, Canada

Accepted 2019 July 12. Received 2019 July 10; in original form 2019 April 18

ABSTRACT

We investigate the possibility of measuring intergalactic magnetic fields using the dispersion measures and rotation measures of fast radio bursts. With Bayesian methods, we produce probability density functions for values of these measures. We distinguish between contributions from the intergalactic medium, the host galaxy, and the local environment of the progenitor. To this end, we use constrained, magnetohydrodynamic simulations of the local Universe to compute lines-of-sight integrals from the position of the Milky Way. In particular, we differentiate between predominantly astrophysical and primordial origins of magnetic fields in the intergalactic medium. We test different possible types of host galaxies and probe different distribution functions of fast radio burst progenitor locations inside the host galaxy. Under the assumption that fast radio bursts are produced by magnetars, we use analytic predictions to account for the contribution of the local environment. We find that less than 100 fast radio bursts from magnetars in stellar-wind environments hosted by starburst dwarf galaxies at redshift $z \gtrsim 0.5$ suffice to discriminate between predominantly primordial and astrophysical origins of intergalactic magnetic fields. However, this requires the contribution of the Milky Way to be removed with a precision of $\approx 1 \text{ rad m}^{-2}$. We show the potential existence of a subset of fast radio bursts whose rotation measures carry information on the strength of the intergalactic magnetic field and its origins.

Key words: polarization – galaxies: intergalactic medium – galaxies: magnetic fields – cosmology: large-scale structure of universe – cosmology: observations – radio continuum: general.

1 INTRODUCTION

Fast radio bursts (FRBs) are impulsive bursts in the radio sky of very short duration (0.1–10 ms) with frequencies of about 1 GHz, observed down to 400 MHz (Lorimer et al. 2007). Their observed dispersion measure (DM) exceeds the contribution of the Milky Way (MW), implying an extragalactic origin. Their short duration suggests an emitting region of the order of 100 km, suggesting a neutron star origin. Such a small region only allows for small intrinsic variation of, e.g. the polarization angle, used to observe the Faraday rotation measure (RM), which is directly related to the magnetic field strength along the line of sight (LoS). FRBs are hence potential probes for the intergalactic medium (IGM) and interstellar medium (ISM) in the MW and in the host galaxy, especially in the local environment of the FRB progenitor (see e.g. Zheng et al. 2014;

Keane et al. 2016; Ravi et al. 2016). In this work, we investigate whether FRBs with observed RMs can be used to derive information on the origin of intergalactic magnetic fields (IGMFs).

Currently, the most widely accepted constraints on the comoving strength of magnetic fields in voids stem from observations of the CMB ($B \lesssim 4.4 \times 10^{-9}$ G, Ade et al. 2016) and of TeV-Blazars ($B \gtrsim 3 \times 10^{-16}$ G, Neronov & Vovk 2010), about seven orders of magnitude apart. For a summary of constraints on the magnetic field strength and coherence lengths, see Taylor, Vovk & Neronov (2011) or Dzhatdoev et al. (2018).

A number of processes have been proposed to generate cosmic magnetic fields. Primordial scenarios consider processes in the early Universe, mostly prior to the recombination epoch, e.g. during phase transitions or inflation (e.g. Campanelli 2009; Kahnashvili et al. 2010; Subramanian 2016). Another possible scenario is the generation of magnetic fields during early galaxy formation, e.g. by feedback of active galactic nuclei (AGNs; e.g. Vazza

* E-mail: shackste@physnet.uni-hamburg.de

et al. 2017) or winds from compact galaxies (Kronberg, Lesch & Hopp 1999; Donnert et al. 2009; Dubois & Teyssier 2010). For a detailed overview on the different models, see e.g. Widrow (2002). These two scenarios result in severely different predictions for the magnetic field strengths in voids of the large-scale structure. In reality, it is likely that both the scenarios contribute to the origin of cosmic magnetic fields. Measuring their strength would allow us to put reasonable constraints on the origin of those fields (e.g. Vazza et al. 2017).

Since their first discovery (Lorimer et al. 2007), there has been a large number of studies addressing the nature and origin of FRBs (e.g. Zhang 2014; Ravi & Loeb 2018; Marcote & Paragi 2019), see Katz (2016a), Lorimer (2018), and Petroff, Hessels & Lorimer (2019) for reviews. Ravi et al. (2019) have summarized the expected progress in the coming decade.

So far, two repeating sources have been identified (Scholz et al. 2016; Spitler et al. 2016; CHIME/FRB Collaboration 2019) that rule out cataclysmic scenarios, at least for those events. Many more discoveries are expected in the very near future. Repeating signals allow us to test time dependence of their properties, making them the subject of intensive studies (e.g. Lu, Kumar & Narayan 2018; Hessels et al. 2019; Houben et al. 2019; Li et al. 2019; Lyutikov 2019; Yang, Zhang & Zhang 2019).

Still, very little is known about the population and origin of FRBs (e.g. Caleb, Spitler & Stappers 2018; Katz 2018; Palaniswamy, Li & Zhang 2018; Caleb et al. 2019; James 2019). To keep track of all the different models, they are collected in the living theory catalogue of FRBs (Platts et al. 2018). Here, we investigate the application of FRBs as probes of cosmic magnetism, with a few priors on their possible origin. We present a framework that can be used to compare observations to theory to make quantitative inferences.

At this point, only a few FRBs have observed RMs. Once the next generation of telescopes, such as e.g. CHIME/FRB, FAST, MeerKat, and SKA, begin their surveys, this number is expected to increase drastically (Jonas 2009; Nan et al. 2011; Keane, Fender & Hassall 2013; Macquart et al. 2015; The CHIME/FRB Collaboration 2018).

Akahori, Ryu & Gaensler (2016) produced predictions for the intergalactic DM_{IGM} and RM_{IGM} of FRBs from the IGM. They use numerical simulations for the large-scale structure and the IGMF to test whether combining both measurements yields information on IGMFs. Their results show that the RM is dominated by the hot gas in clusters while the dominant contributor to DM changes with redshift. Still, they show that the radial component of the density-weighted IGMF strength in filaments can be inferred from combined measurements within a factor of ~ 2 .

Vazza et al. (2018) investigate the variance in RM_{IGM} due to the assumed magneto-genesis model. They assume astrophysical or primordial origin of cosmic magnetic fields, similar to the models used in this work. For FRBs located at a redshift of $z = 1$, they find differences in $\langle \text{RM}_{\text{IGM}} \rangle$ between the models of about one order of magnitude. In principle, this allows us to draw conclusions on the strength of the IGMF. However, it is unclear at which redshift the observed signal reveals most information.

Walker, Ma & Breton (2018) provide a framework similar to the one presented in this paper. They obtain predictions of DM in the form of likelihood functions for the different contributing regions. They use these to derive estimates on the redshift of FRBs, which mostly agree with $z \approx 0$ in the lower bounds. Thus, they conclude that the observed DM_{obs} can only be used to infer an upper limit on the redshift. This is in agreement with several other studies on that topic (Dolag et al. 2015; Luo et al. 2018; Niino 2018; Pol et al.

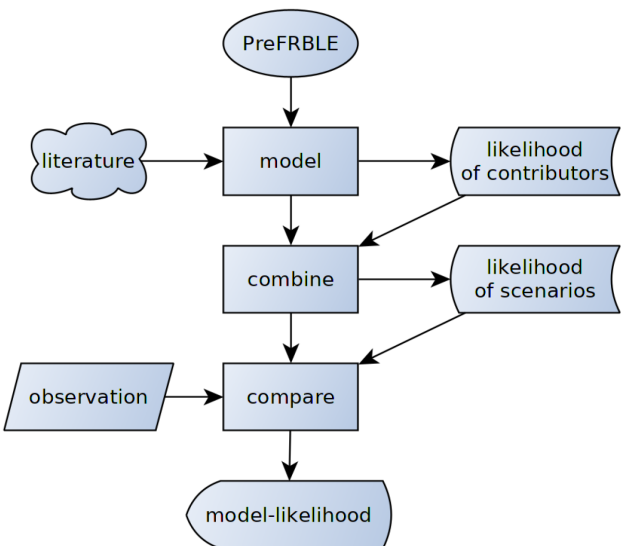


Figure 1. Flowchart to depict the basic structure of the inference presented in this work. We use results in the literature to model the contributions to DM and RM from different regions along the LoS of FRBs. These results are combined to predict the full measures expected at the Earth in different scenarios for the combination of contributor models. Finally, the results are compared to observational data to quantify and compare the posterior likelihood of several scenarios to produce the observed data.

2019). We note that the framework presented here easily allows one to infer the redshift of an FRB from its DM, similar to the findings of Walker et al. (2018) and Pol et al. (2019). However, our results are subject to the same uncertainties and cannot improve on previous results.

In this work, we show how to combine predictions of DM and RM for different regions along the LoS of FRBs and to compare them to the observed DM_{obs} and RM_{obs} in order to study the IGMF. Fig. 1 shows an overview of the basic structure of the inference.

We improve on previous studies by use of constrained simulations of the local Universe that resemble different scenarios of magnetogenesis, and further, by comparing the individual contributions to DM and RM along the LoS, considering redshifts out to $z = 6$.

This paper is organized as follows. In Section 2, we explain how we model the different contributions to DM and RM along the LoS of FRBs and how to compute their likelihood functions. In Section 3, we discuss the results of the individual models of the contributing regions. In Section 4, we combine the predictions of all contributors to predict observed DM_{obs} and RM_{obs}. We show how these can be used to interpret DM_{obs} and RM_{obs} regarding the origin of IGMFs. Finally, in Section 5 we discuss our results and in Section 6 we conclude.

2 MODELS

In this section, we describe the models investigated in this work and how we obtain the likelihood functions. A summary of all models can be found in Table 1.

2.1 Intergalactic medium

2.1.1 Model

We model the IGM using constrained magnetohydrodynamic (MHD) simulations of the local Universe, produced with the ENZO

Table 1. Summary of all models investigated in this work. n_{FRB} is the assumed number density of possible progenitor positions, and n_{\star} is the number density of stars in the MW. NE2001 stands for the density model of thermal electrons in the MW presented in Cordes & Lazio (2002). JF12 stands for the magnetic field model of the MW developed by Jansson & Farrar (2012).

Mnemonic	Physics
IGM:	
Primordial	3D-MHD model of the local Universe with strong uniform initial magnetic field of $B_0 = 1 \text{ nG}$ comoving
Astrophysical	3D-MHD model of the local Universe with very weak initial magnetic field and magnetic feedback of an AGN
Host galaxy:	
Uniform	MW-like spiral galaxy model (NE2001 and JF12), $n_{\text{FRB}} = \text{const.}$
Star density	MW-like spiral galaxy model (NE2001 and JF12), $n_{\text{FRB}} \propto n_{\star}$
Dwarf	Starburst dwarf galaxy similar to IC10 or host of FRB121102, $n_{\text{FRB}} \propto n_{\star}$
Local environment of progenitor:	
Uniform	Magnetar in uniform ISM environment
Wind	Magnetar in environment dominated by stellar winds of seed star
Wind+SNR	Wind plus contributions of SNR
Milky Way:	
NE2001 + JF12	Best-fitting model for Galactic RM (NE2001 and JF12)

code (Bryan et al. 2014). The simulations start from initial conditions obtained from a procedure summarized by Sorce et al. (2016). The constraints applied in order to reproduce the local Universe at $z = 0$ are fully described by Tully et al. (2013). Simulations have been produced within the Planck cosmology framework ($\Omega_m = 0.307$, $\Omega_\Lambda = 0.693$, $h = 0.677$, $\sigma_8 = 0.829$, Planck Collaboration I 2014). Further information on the models can be found in Hackstein et al. (2018), where they have been investigated in the context of propagation of cosmic rays. The three-dimensional data sets at $z = 0$ are also publicly available at <https://crpropa.desy.de/> under ‘Additional resources’.

We consider two different scenarios for the predominant genesis of IGMFs, *primordial* versus *astrophysical*. To do so, we make use of the result of a single simulation, which considers the *primordial* origin of IGMFs. From that and from the *astrophysical* model presented in Hackstein et al. (2018), we extract the $|B| \propto \rho$ relation in Fig. 2 (cf. Vazza et al. 2017). The difference in $|B|(\rho)$ between the two models is most prominent at very low density, far away from the central cluster regions, where most AGNs reside. However, the contribution from these regions to the RM is likely far below the ionospheric foreground $\approx 1 \text{ rad m}^{-2}$, hence not observable. The most interesting regions are the vicinity of clusters, filaments, and other regions, where $1 < \rho / \langle \rho \rangle < 200$.

The *primordial* model starts with a uniform magnetic field with comoving magnetic field strength $B_0 = 1 \text{ nG}$, slightly below upper limits of the PLANCK collaboration, $B_0 \lesssim 4.4 \text{ nG}$ (Ade et al. 2016). Note that Trivedi, Subramanian & Seshadri (2014) derived an upper limit of $B_0 \lesssim 0.6 \text{ nG}$ using the CMB Trispectrum. The *astrophysical* model is initialized with a $B_0 = 10^{-8} \text{ nG}$. Though this is below the lower limits obtained for present fields in voids, the final result of the simulation agrees with that limit, $B_{\text{void}} \gtrsim 3 \times 10^{-7} \text{ nG}$ (Neronov & Vovk 2010). In order to obtain magnetic fields that agree with observations of clusters, this model allows for additional seeding of magnetic fields by feedback of AGNs below redshift 4. In order to obtain results for the *astrophysical* model from the data of *primordial*, we apply the ratio of average $|B|(\rho)$ for these two models as correction factor on the magnetic field outside of galaxy clusters, where cosmic gas density $\rho < 200 \langle \rho \rangle$. This allows us to test different prescriptions for three-dimensional magnetic fields in our cosmological volume with a limited consumption of computing

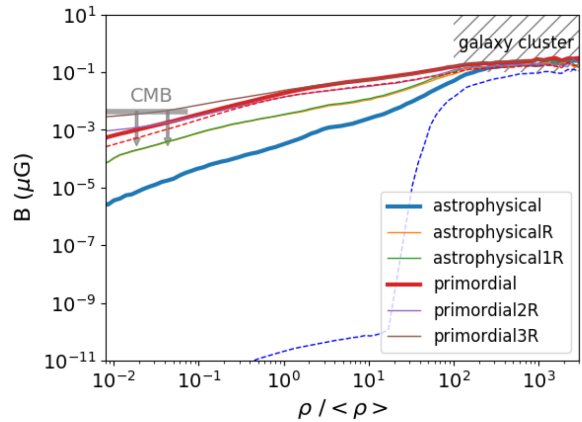


Figure 2. Relation between average magnetic field strength B and gas density ρ in the different IGM models investigated in Hackstein et al. (2018). The two models used in this paper are drawn with thick lines. The dashed lines show results for the median of B , instead of the mean. We indicate the range of magnetic fields in clusters (e.g. Feretti et al. 2012) as well as the upper limit of fields in voids according to CMB observations by PLANCK, $B_0 \lesssim 4.4 \text{ nG}$ (Ade et al. 2016).

time. However, in this work we investigate only two models at the extreme ends of possible strengths of the IGMF in order to see whether FRBs carry any information on the IGMF.

Note that the average of $|B|$ is dominated by the high values in a density bin. The median, shown as dashed lines in Fig. 2, reflects much better the huge difference in the magnetic field outside high-density structures. Using the median ignores possible high values of $|B|$ within a density bin, hence underestimates the magnetic field and the RM. The average instead is dominated by these high values and forces the magnetic field to values of similar strength, everywhere within the density bin. In this case, the results for the *astrophysical* model are much closer to the *primordial*, representing the most pessimistic case to tell the two extreme models apart. Hence, the use of the average instead of the median strengthens the conclusion that the observation of FRBs can be used to distinguish between these two models.

We note, however, that the *primordial* model we probe here is initialized with a uniform field, whose topology is preserved in low-density regions. This can affect the distribution of RM from FRBs in the local Universe, making smaller values less probable. This is because the contributions from different parts of the IGM are less likely to cancel out each other. In Appendix A, we investigate how that influences the final results and find a negligible impact on observable $\text{RM}_{\text{obs}} \gtrsim 1 \text{ rad m}^{-2}$ (see also Vazza et al. 2018).

The use of numerical simulations will improve our results over those of Walker et al. (2018) and Niino (2018) by accounting for the uncertainty that arises due to inhomogeneities in the IGM. Like Akahori et al. (2016), we apply the usual method of cosmological data stacking (e.g. da Silva et al. 2000). We reconstruct the cosmic space from redshift $z = 0$ to 6 with use of simulation outputs at redshifts $z = 0.0, 0.2, 0.5, 1.5, 2.0, 3.0$, and 6.0. The LoS starts at redshift $z = 6$ and traverses the simulated volume in a randomly oriented rectilinear path. When the LoS reaches the corresponding redshift, the trajectory is continued in the next snapshot. The final snapshot at $z = 0$ is used from half the cosmic time towards the previous snapshot at $z = 0.2$. Finally, all values are corrected for a smooth evolution with redshift.

The DM_{IGM} for a LoS with cosmological distance is

$$\text{DM}_{\text{IGM}} = \int_0^{d_{\text{FRB}}} (1+z)^{-1} \left(\frac{n_e}{\text{cm}^{-3}} \right) \left(\frac{\text{dl}}{\text{pc}} \right) \text{pc cm}^{-3}, \quad (1)$$

where d_{FRB} is the comoving distance to the FRB source and n_e is the proper thermal electron density (Xu & Han 2015). DM measures the extra traveltimes of radiation at low frequencies due to dispersive effects in plasma. Hence, it scales with redshift as $\text{DM} \propto (1+z)^{-1}$.

The RM_{IGM} for a LoS with cosmological distance is

$$\text{RM}_{\text{IGM}} = \frac{\Delta\Phi}{\Delta\lambda^2} \approx 0.81 \int_{d_{\text{FRB}}}^0 (1+z)^{-2} \left(\frac{B_{\parallel}}{\mu\text{G}} \right) \left(\frac{n_e}{\text{cm}^{-3}} \right) \times \left(\frac{\text{dl}}{\text{pc}} \right) \text{rad m}^{-2}, \quad (2)$$

where B_{\parallel} the proper magnetic field component parallel to the LoS (Xu & Han 2014). RM is the ratio of relative rotation of polarization angles Φ at different frequencies divided by the difference of the squared wavelength λ . The former is not affected by cosmic expansion, therefore RM scales with redshift as $\text{RM} \propto (1+z)^{-2}$.

The free electron density, n_e , is computed assuming full ionization and a mean molecular weight $\mu_e \approx 1.16$ of an electron for cosmic fractions of hydrogen and helium.

2.1.2 Likelihood function

We obtain the likelihood function of the IGM contribution from LoS integrals. These are produced using the `LIGHTRAY` function of the `TRIDENT` package (Hummers, Smith & Silvia 2017). This function extracts field values from data cells intersected by a LoS, defined by start and end positions in the three-dimensional volume. It also computes the redshift that reflects the distance to the observer. This way, it allows us to compute the redshift-corrected values along the LoS that contribute to the DM and RM.

These LoSs start from the position of the MW, defined as the centre of the box in our constrained simulation of the local Universe. They progress in evenly distributed directions defined by the `HEALPIX` (Górski et al. 2005) tessellation of the sphere (similar to Stasyszyn et al. 2010). We use a total of 49 152 LoSs, corresponding to a pixel radius of $1\text{--}2'$. This allows us to resolve local structures while computation costs are kept at a minimum. The

total computation took about 1200 h of CPU time. Differences in the likelihood function are <0.1 per cent compared to the next smaller tessellation of the sky with 12 288 LoSs. Hence, the likelihood function is reasonably converged.

The total path-length of the LoS exceeds the size of the constrained high-resolution portion of our simulation volume, which is the central (250 Mpc)³. Therefore, direction-dependent results beyond the first crossing of this region would be misleading. Instead, for results at higher redshifts ($z \gtrsim 0.1$) we investigate a statistical sample of LoS with random orientation. These are obtained by stacking segments between random points taken from the constrained regions, until the LoS reaches the redshift of the current snapshot. The process continues with the next snapshot, until the full LoS is built. The final snapshot of the simulation is at $z = 0$ and would not be used in the procedure described above. Hence, it is used until half of the cosmic time towards the next snapshot at $z = 0.2$, where $z \approx 0.9$. The fact that $\nabla \cdot \vec{B}$ is not conserved to 0 at the interfaces where we combine different segments of the LoS does not pose any problem for our analysis, as <1 per cent of cells are affected by this problem.

The likelihood function is proportional to the amount of LoSs that deliver the same value. Assuming an isotropic distribution of FRBs in the sky, the calculation is straightforward:

$$p(\text{DM}'|z) = \frac{\oint \delta(\text{DM}(\theta, \phi; z) - \text{DM}') d\theta d\phi}{\oint d\theta d\phi} \approx \frac{N_{\text{DM}'}}{N_{\text{tot}}}, \quad (3)$$

where $N_{\text{DM}'}$ is the number of LoSs from a redshift z with $\text{DM} \approx \text{DM}'$, and N_{tot} is the total number of LoSs from that redshift. The same holds for the RM.

2.2 Host galaxy

2.2.1 Model

To highlight the influence of host galaxies, we investigate two different types of galaxies, a spiral galaxy similar to the MW and a starburst dwarf galaxy similar to the host of FRB121102. We note that this small number of models does not suffice to reflect the variety of different galaxies that are likely to host FRBs, but gives a rough estimate on the range of possible contributions.

Integrating the galaxy stellar mass function (Baldry et al. 2012) yields that 68 per cent of stars reside in galaxies of $10^{11}\text{--}10^{12} \text{ M}_{\odot}$, similar to the MW. Such galaxies are likely hosts, if FRBs are produced by magnetars (e.g. Popov & Postnov 2010; Katz 2016b; Beloborodov 2017; Metzger, Berger & Margalit 2017; Metzger, Margalit & Sironi 2019). We obtain predictions for the spiral host galaxy with use of the NE2001 model (Cordes & Lazio 2002) for the thermal electron density, combined with the JF12 model (Jansson & Farrar 2012) for the magnetic field, where we use the best-fitting parameters for the MW. Luo et al. (2018) compared the results of NE2001 with the model of Yao, Manchester & Wang (2017) and found that the overall statistics are rather similar, NE2001 tending to slightly higher values of DM. Here we exclusively use the NE2001 model, which was also assumed by Jansson & Farrar (2012).

Though it has been argued that the NE2001 model is not good enough to exactly reconstruct the DM foreground of pulsar data (see Xu & Han 2015), it is a reasonable choice to obtain a decent statistical estimate. Calculations have been performed using the HAMMURABI code (Waelkens et al. 2009), which computes the LoS integrals in evenly distributed directions on the whole sky seen from a given position to the edge of the galaxy model.

The likelihood of a given value of DM_{host} and RM_{host} from the host highly depends on the position of the progenitor within the host, which is uncertain. To account for that, a reasonable choice is to sample different possible positions and combine their predictions. The positions are drawn randomly, following a probability density that we assume to be either uniform or proportional to the star density. In particular, for the latter we use the combination of a thick disc and a thin disc of radius R_i and scale height Z_i with exponentially falling star density

$$n_{\text{star}}(R, Z) \propto \exp\left(-\frac{R}{R_i} - \frac{|Z|}{Z_i}\right), \quad (4)$$

using the best-fitting parameters obtained for distribution of M dwarfs in the MW, i.e. $R_{\text{thick}} = 3.6$ kpc, $Z_{\text{thick}} = 0.9$ kpc, $R_{\text{thin}} = 2.6$ kpc, and $Z_{\text{thin}} = 0.3$ kpc (Jurić et al. 2008).

Dwarf irregular galaxies in a starburst phase, which we will refer to as starburst dwarf galaxies hereafter, have high star formation rates, hence their stellar population is relatively young. Magnetars have short lifespans, $\approx 10^4$ yr (e.g. Beniamini et al. 2019), and are produced by massive stars, 20–45 M_{\odot} (Chabrier 2003), that have rather short lifetimes, $\sim 10^7$ yr (e.g. Wit et al. 2005). This makes starburst dwarf galaxies a likely host for FRBs produced by magnetars.

The first localized FRB121102 was indeed found to reside in such a starburst dwarf galaxy, having a high star formation rate, low metallicity, and no AGN (Chatterjee et al. 2017; Tendulkar et al. 2017). Low-mass and low-metallicity galaxies with high star formation rates were also found to be overrepresented hosts of gamma-ray bursts and superluminous supernovae at low redshift (e.g. Fruchter et al. 2006; Vergani et al. 2015; Perley et al. 2016).

A well-studied starburst dwarf galaxy in the local Universe is IC 10, which is at 0.8 Mpc distance. It is the only member of the Local Group that is currently in the starburst phase. Its properties are very similar to that of the host of FRB121102 (e.g. Richer et al. 2001; Leroy et al. 2006; Magrini & Gonçalves 2009). We use the magnetic field model of Heesen et al. (2011), who studied IC 10 with radio continuum polarimetry, to estimate the possible RM contribution of a starburst dwarf galaxy. We assume a constant thermal electron density n_e in the galactic mid-plane, which falls off exponentially with height. For the magnetic field, a combination of a spiral plane-parallel field and a poloidal vertical field both with a characteristic strength B_{host} is used. We neglect random components of the magnetic field since they do not significantly affect the distribution of RM. The distribution of stars in dwarf galaxies is centred on the disc. We model their distribution with an exponential with a scale height of 300 pc (similar to Leroy et al. 2006, who studied IC 10).

2.2.2 Likelihood function

Within the MW-like spiral galaxy, we draw a sample of possible positions of the progenitor, according to the assumed distribution function. Tests showed that 1000 positions are enough to ensure converged results. For each of these positions, we compute the full sky of DM_{host} and RM_{host} measurements, similar to the approach used by Walker et al. (2018). The LoS integral is then computed to the edge of the host in all different directions defined by the HEALPix (Górski et al. 2005) tessellation of the sphere. The probability density of values on the full sky delivers the likelihood functions $P(\text{DM}_{\text{host}})$ and $P(\text{RM}_{\text{host}})$. The sum of the likelihood functions at the different positions is then the full likelihood function for the host galaxy.

Note that the results at the position of the Sun can be used to obtain predictions for the contribution from the MW itself. By construction, the results are identical to results in Jansson & Farrar (2012).

For the starburst dwarf galaxy, we compute LoS integrals for different inclination angles and penetration depths, such that the assumed distribution of FRBs in the host is constant throughout the disc. Since the model is rotationally invariant, variations of the azimuthal angle are redundant. LoSs are calculated until they leave the disc, excluding contributions of the galactic halo, which, however, is expected to be at least one order of magnitude below the galactic contribution.

To account for possible variance across the distribution of similar starburst dwarf galaxies, we combine predictions for several choices of n_e and B_{host} , according to prior distributions explained in detail in Appendix B.

The dispersion delay produced at the host increases, due to cosmic expansion. The observed contribution of DM_{host} to the total DM_{obs} scales with the source redshift as $(1+z)^{-1}$ (e.g. Macquart et al. 2015), so the likelihood function shifts accordingly (Walker et al. 2018) as

$$p(\text{DM}_{\text{host}}|z_s) = (1+z_s)p((1+z_s)\text{DM}_{\text{host}}|z_0). \quad (5)$$

For $\text{RM} = \frac{\Delta\Phi}{\Delta\lambda^2}$, the contribution of the host scales with $(1+z)^{-2}$ instead. Therefore, the corresponding likelihood function shifts as

$$p(\text{RM}_{\text{host}}|z_s) = (1+z_s)^2 p((1+z_s)^2 \text{RM}_{\text{host}}|z_0). \quad (6)$$

2.3 Local environment

2.3.1 Model

We assume FRBs to be produced by magnetars (e.g. Popov & Postnov 2010; Pen & Connor 2015; Katz 2016b; Beloborodov 2017; Metzger et al. 2017; Metzger et al. 2019). Neutron stars are generally considered one of the most likely sources for FRBs. Beniamini et al. (2019) concluded that 12–100 per cent of neutron stars are born as magnetars. Hence, it is expected that they are numerous around star-forming regions. Their number density scales with the star formation rate. Results of Niino (2018) and Locatelli et al. (2019) suggest that the number density of FRBs does also scale with the star formation rate. This makes magnetars a likely candidate for the source of FRBs. Many other objects have been proposed as sources of FRBs (see Platts et al. 2018, who provide a living catalogue of theories). We restrict this study to exemplarily compare two models of the local environment of the FRB progenitor.

To account for the local environment of a magnetar FRB progenitor, we make use of the models and results of Piro & Gaensler (2018). They give theoretical predictions for the DM_{prog} and RM_{prog} from the local environment of the FRB, assuming they are produced by a young neutron star. They consider two models. One model assumes a uniform local ISM, while the other accounts for changes in the ISM due to stellar winds of the seed star.

In this work, we consider the two models for the *uniform* and *wind* cases, plus we consider the additional contribution of the SNR environment for the latter model in the *wind+SNR* case. We use this low number of models to show how multiple progenitor models can be compared and combined to be tested against observations.

Stellar winds cause the magnetic field of the local environment to align and form a significant large-scale component. The RM predictions for that environment in the *wind* model are thus much more robust than for the supernova remnants. The latter model

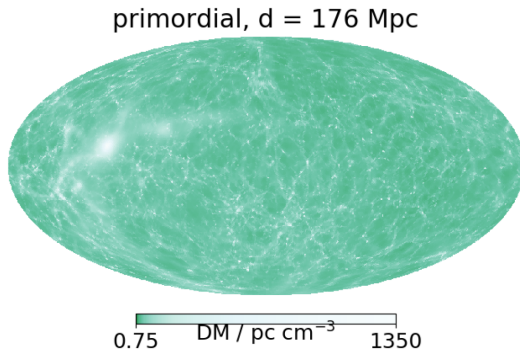


Figure 3. Full-sky map of DM_{IGM} predictions for sources at 176 Mpc distance in the local Universe. Results are shown in supergalactic coordinates for the *primordial* model. The distribution of free electrons, hence DM , is identical to the *astrophysical* case.

assumes the shock-generated magnetic field to be coherent, while the topology is very likely random. Hence, results for the *uniform* and the *wind+SNR* model should be considered as upper limits.

2.3.2 Likelihood function

Under the assumption that FRBs are produced at young neutron stars, Piro & Gaensler (2018) have derived expectation values for the DM_{prog} and RM_{prog} of the local FRB environment. These are given as functions of the ISM number density n_{ISM} , the time since the SN t , the energy of the explosion E , the mass of SN ejecta M , the wind mass-loading parameter K , the stellar radius R_* , and the stellar magnetic field B_* .

The likelihood function is obtained with a Monte Carlo method, where we sample these parameters with reasonable prior distributions, calculate the corresponding DM_{prog} and RM_{prog} , and compute their probability density. The priors chosen to obtain those are summarized in Appendix B.

The contribution from the progenitor undergoes the same evolution with redshift as the contribution from the host, see equations (5) and (6).

3 MODEL RESULTS

3.1 IGM, constrained results for the local Universe

3.1.1 Dispersion measure

In Fig. 3, we show the full-sky projection of the expected DM_{IGM} of FRBs at a distance of 176 Mpc. This nicely shows the distribution of structure in the local Universe (see Hackstein et al. 2018). The Virgo cluster is the most dominant local contributor with up to $\text{DM}_{\text{IGM}} \gtrsim 10^3 \text{ pc cm}^{-3}$.

The DM_{IGM} prediction is the same in both IGM models, as they result in almost identical distribution of gas.

Taken from such full-sky maps at different redshifts, in Fig. 4 we present the evolution of the likelihood function of DM_{IGM} . These results agree reasonably well with results in Dolag et al. (2015) and Walker et al. (2018). At short distances, the tail at high values is more pronounced, caused by nearby, high-density regions. With increasing distance, the distribution moves towards a log-normal distribution, the mean of which increases steadily due to the cumulative growth of DM_{IGM} . Also, an increasing number of LoS crosses high-density structures, which add to the tail at high values.

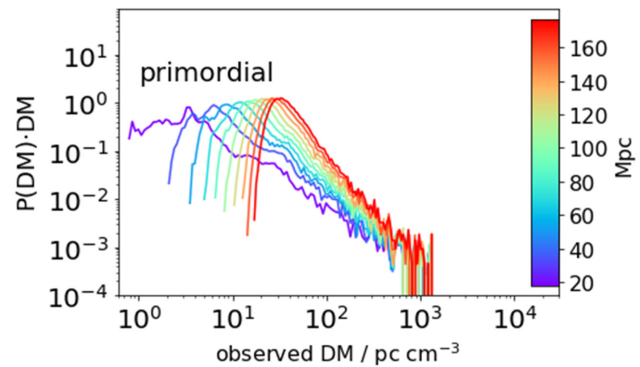


Figure 4. Likelihood function $P(\text{DM}_{\text{IGM}} | d)$ for FRB sources at distance d in the local Universe, $d \lesssim 176$ Mpc, for the *primordial* model. The distribution of free electrons, hence DM , is identical to the *astrophysical* case.

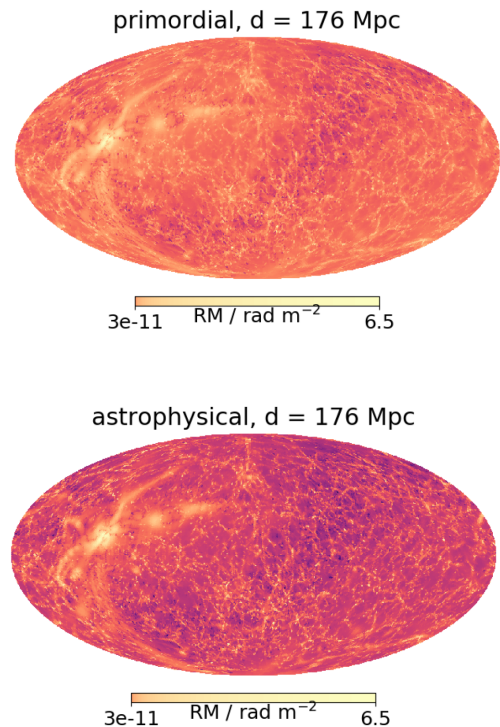


Figure 5. Full-sky map of $|\text{RM}_{\text{IGM}}|$ predictions for sources at 176 Mpc distance in the local Universe, for the *primordial* (top) and *astrophysical* models (bottom). Results are shown in supergalactic coordinates.

3.1.2 Rotation measure

In Fig. 5, we show the full-sky projection of expected RM_{IGM} of FRBs at a distance of 176 Mpc for both the *primordial* and *astrophysical* models. The structure of the local Universe is nicely reproduced. Again, the Virgo cluster appears as the most dominant contributor with up to $|\text{RM}_{\text{IGM}}| \gtrsim 6 \text{ rad m}^{-2}$, which roughly agrees with the observations of Vallée (1990).

Both IGM models result in almost identical maximum values of RM_{IGM} . These are found in LoSs that pass through regions of high density, like the Virgo cluster, that contribute very high values of RM_{IGM} . The models were built to reproduce the conditions observed in these regions in the local Universe. However, the two

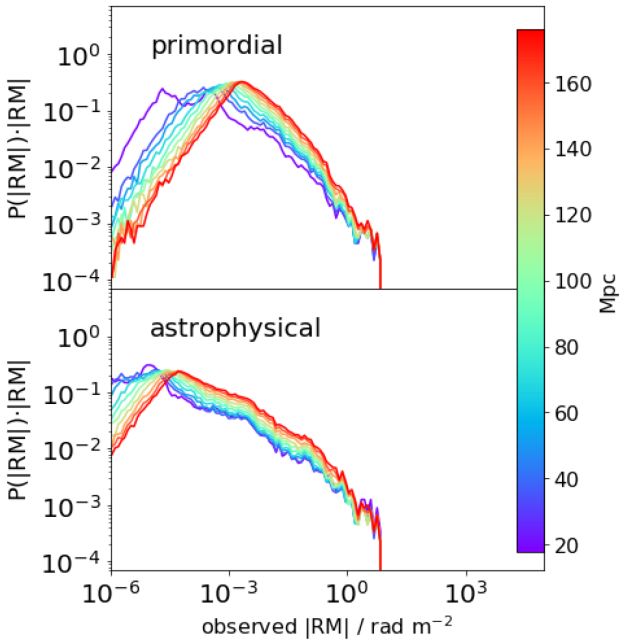


Figure 6. Likelihood function $P(|\text{RM}_{\text{IGM}}| | d)$ for FRB sources at distance d in the local Universe, $d \lesssim 176$ Mpc for the *primordial* (top) and *astrophysical* models (bottom).

magneto-genesis scenarios result in severely different magnetic fields in voids. Fig. 5 shows that LoSs that do not pass through regions of high density have RM_{IGM} lower by up to two orders of magnitude.

Taken from such full-sky maps at different redshifts, in Fig. 6 we present the evolution of the likelihood function of RM_{IGM} . Since the distribution of positive and negative values is very similar, we make use of $\log(|\text{RM}|)$ in all our likelihood functions to compare contributions of different orders in more detail.

The highest values, $\text{RM}_{\text{IGM}} \approx 1\text{--}10 \text{ rad m}^{-2}$, agree in both models. These are LoSs that intersect high-density regions, associated with the $\rho/\langle\rho\rangle \geq 10^2$ overdensity of galaxy clusters, contributing high values of RM_{IGM} . However, the fraction of such LoSs is limited, and they do not affect much the overall distribution of RM_{IGM} (Vazza et al. 2018).

As the peak increases with distance, the *astrophysical* case peaks about two orders of magnitude below the *primordial* case. However, the overall contribution of RM_{IGM} is much too low to have significant influence on the total RM_{obs} within maximum distance in the constrained volume, 176 Mpc. This also holds for possibly different results for positive and negative RM_{IGM} caused by dense structure outside of cores of clusters.

Note that the *primordial* model started from a magnetic field that was coherent over the whole simulation volume. Outside of dense structures, this topology of the initial field is conserved and results in very optimistic estimates of RM_{IGM} , as contributions from separate parts of the LoS cannot cancel each other. A more detailed study of this effect can be found in Appendix A. Note that for the constrained distance, this feature is of the order of $10^{-2} \text{ rad m}^{-2}$ in the *primordial* case, subdominant to other contributions along the LoS and hence not observable. At greater distances, we combine separate trajectories with random orientations, thus enabling the contributions from separate sections of the LOS to cancel each other.

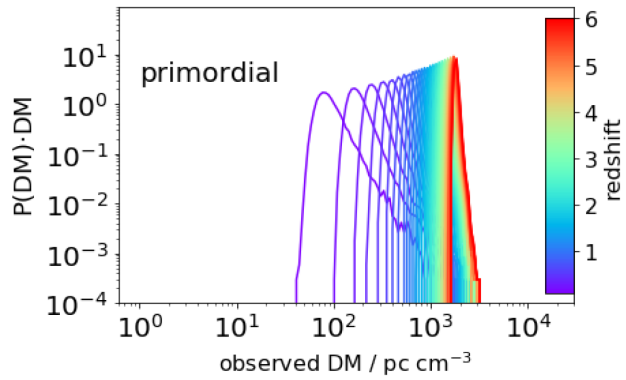


Figure 7. Likelihood function $P(\text{DM}_{\text{IGM}} | z)$ for FRB sources at redshift z in the distant Universe for the *primordial* model. The distribution of free electrons, hence DM, is identical to the *astrophysical* case. From blue to red, the graphs show results at redshifts $z = 0.1\text{--}6.0$ in steps of 0.1.

3.2 IGM, high-redshift results

3.2.1 Dispersion measure

In Fig. 7, we present the resulting likelihood function of DM_{IGM} contribution from the IGM for FRB at different redshifts in the distant Universe for the *primordial* model. The distribution of free electrons, hence DM, is identical to the *astrophysical* case. The distribution of DM_{IGM} ($z = 1$) is very peaked around 1000 pc cm^{-3} , in good agreement with results of previous studies, where this value is reported to be $855\text{--}1200 \text{ pc cm}^{-3}$ (Ioka 2003; Inoue 2004; McQuinn 2013; Deng & Zhang 2014; Dolag et al. 2015; Walker et al. 2018; Pol et al. 2019). The shape is similar to the results in Fig. 4 at the highest distance and compares well with the results of Dolag et al. (2015) and Walker et al. (2018).

With increasing redshift, the proper density of free electrons increases, as does the average DM_{IGM} contribution of the IGM. This makes the whole likelihood function $P(\text{DM}_{\text{IGM}})$ shift to higher values with increasing redshift. As the cumulative growth of DM_{IGM} from low-density regions approaches the scale of dense structure contributions, $P(\text{DM}_{\text{IGM}})$ becomes much narrower. However, the overall change is slower at higher redshift z (Zheng et al. 2014). Therefore, the likelihood function for high DM_{IGM} is much broader in z . This shows that, although the DM delivers good upper limits on z , the uncertainties in the estimate will always remain rather large, and other ways to infer z , e.g. by identification of the host, are preferred (cf. Dolag et al. 2015; Walker et al. 2018; Kumar & Linder 2019; Pol et al. 2019).

3.2.2 Rotation measure

In Fig. 8, we present the likelihood function of RM_{IGM} contribution from the IGM for FRB at redshift z in the *primordial* and *astrophysical* models of the distant Universe. As the models used here were produced with the same tools and physics as the ones used by Vazza et al. (2018), the results we find are quite similar. However, the average value of these distributions is significantly lower than the results of Akahori et al. (2016), which is due to the lower magnetic field strength outside of clusters. Here we use $B \sim 0.1 \text{ nG}$ instead of the $10\text{--}100 \text{ nG}$ of Akahori et al. (2016), due to the more efficient dynamo amplification assumed in the latter model.

At lower redshifts, $z \sim 0.1$, RM_{IGM} tends to low values close to zero. Only a few LoSs show high values of up to $\text{RM}_{\text{IGM}} \sim 100 \text{ rad m}^{-2}$.

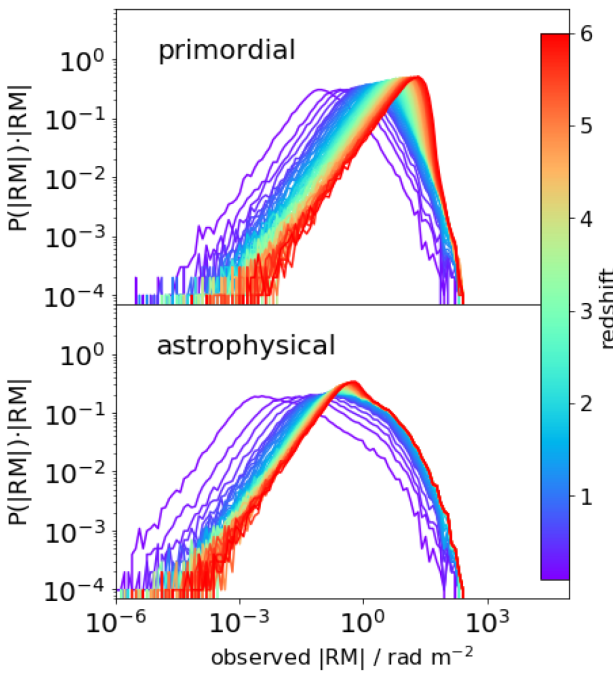


Figure 8. Likelihood function $P(\text{RM}_{\text{IGM}}|z)$ for FRB sources at redshift z in the distant Universe in *primordial* (top) and *astrophysical* (down) models. From blue to red, the graphs show results at redshifts $z = 0.1$ – 6.0 in steps of 0.1.

m^{-2} . These are LoSs that traverse high-density regions, associated with the $\rho/\langle \rho \rangle \geq 10^2$ overdensity of galaxy clusters, which contain amplified magnetic fields. With higher redshift, more and more LoS traverse clusters, some even twice, and their RM_{IGM} reach values above 100 rad m^{-2} in both the *primordial* and *astrophysical* cases.

Many of the LoSs traverse the low-density IGM only and contribute most of RM_{IGM} . The cumulative growth shifts RM_{IGM} to higher values, but slower than DM_{IGM} , as RM_{IGM} from different regions of the IGM can cancel each other.

The IGM model we used considers an initial magnetic field that is coherent over 250 Mpc h^{-1} , i.e. the full simulation volume. This is well conserved in low-density regions and results in a uniform sign of RM_{IGM} contributions along a continuous LoS segment. However, since several of these segments with random orientation are combined to obtain the full LoS, they can cancel each other and we obtain results that are statistically equivalent to a stochastic field with lower coherence length.

There is a significant difference in $P(\text{RM}_{\text{IGM}}|z)$ between the *primordial* and *astrophysical* cases. The peak of RM_{IGM} is two orders of magnitude lower in the latter case, similar to results at low redshift, shown in Fig. 6. Further, the shape looks increasingly different at higher redshift z . Though the peak value is rather low, $\lesssim 10 \text{ rad m}^{-2}$ still at $z = 6$, the different shapes will likely reflect in the distribution of extragalactic RM_{EG} , given that there is no dominant contribution from the other regions.

3.3 Progenitor environment, host galaxy, and MW

3.3.1 Dispersion measure

The likelihood functions of DM for all models investigated in this work are presented at redshift $z = 1$ in Fig. 9.

The two models for the IGM, *primordial* and *astrophysical*, have identical DM_{IGM} by construction. The two behaviours overlap each other. The dominant peak is at around 10^3 pc cm^{-3} .

The model that assumes a spiral host galaxy similar to the MW is modelled with two distribution functions of the position of the FRB progenitor, one is *Uniform* and the other follows the *star density* in the MW. The bulk of both of these distributions is similar to the MW. There is less DM_{host} around 10^3 pc cm^{-3} , since there are less LoSs that traverse big parts of the galaxy. For the *Uniform* distribution, a lot of progenitors are located close to the border of their host. A huge number of LoSs traverse only small parts of the galaxy. Therefore, the tail towards lower values is much more pronounced.

Xu & Han (2015) also investigate a spiral galaxy. The maximum, $\approx 1500 \text{ pc cm}^{-3}$, and most probable values, $\approx \text{few pc cm}^{-3}$, are similar to our results.

The likelihood function for starburst *dwarf* galaxies as FRB hosts shows a flat plateau at $\text{DM}_{\text{host}} = 1$ – 10^3 pc cm^{-3} due to the assumed flat prior. In most cases, the contribution will be significantly lower than the IGM. However, there is a small probability of a few per cent that it contributes more to the DM_{EG} .

The *uniform* model described by Piro & Gaensler (2018) strongly depends on the ISM density n_{ISM} . The shape of the likelihood function is almost identical to the chosen prior distribution $\pi(n_{\text{ISM}})$. Of course, this depends on the host galaxy and we will show below the result for both host galaxy models investigated in this work.

For the case of MW-like spiral galaxies, we see in Fig. 9 that the supernova remnants can provide an observed DM_{prog} up to several 10^3 pc cm^{-3} , even at a distance of $z = 1$, if the magnetar is located in an HII region. Only the *dwarf* host model has very small chance to contribute similarly high values of DM_{host} . None of the other models is able to produce such high values of DM. This shows how likelihood functions can be used to rule out contributor models for single events and, subsequently, for whole populations.

Fig. 9 also shows that a high DM_{obs} does not necessarily imply a high redshift, but can also be produced in the local environment of the FRB, even if the probability is rather low, $\lesssim 1$ per cent. However, if future observations reveal a significantly higher number of large $\text{DM}_{\text{obs}} \gtrsim 10^3 \text{ pc cm}^{-3}$, this would argue in favour of a population at reasonable cosmic distance, $z \gtrsim 1$.

The *wind* model in Piro & Gaensler (2018) results in a rather flat distribution of DM_{prog} around (10^{-2}) – $(10^{-1}) \text{ pc cm}^{-3}$ that decreases rapidly at both ends. Adding the SNR contribution in *wind+SNR*, the plateau expands to substantially higher values of 10^1 pc cm^{-3} and the tail includes $\text{DM}_{\text{prog}} \gtrsim 10^2 \text{ pc cm}^{-3}$ with a probability of ≈ 0.1 per cent. At redshift $z = 1$, this is far below the IGM contribution.

3.3.2 Rotation measure

Fig. 10 shows the likelihood functions of RM for all models at redshift $z = 1$.

The model for the MW is in agreement with the data provided by Oppermann et al. (2015). The likelihood function is of similar shape as for the IGM, about an order of magnitude above the *primordial* model. It stays above both models of the IGM for all redshifts probed in this work, $z \leq 6$.

The host model that resembles an MW-like spiral galaxy shows a likelihood function for RM_{host} that is very peaked around 10^1 – 10^2 rad m^{-2} – about a magnitude above the peak of the *primordial* model – in case the positions of FRB progenitors scale with the *star*

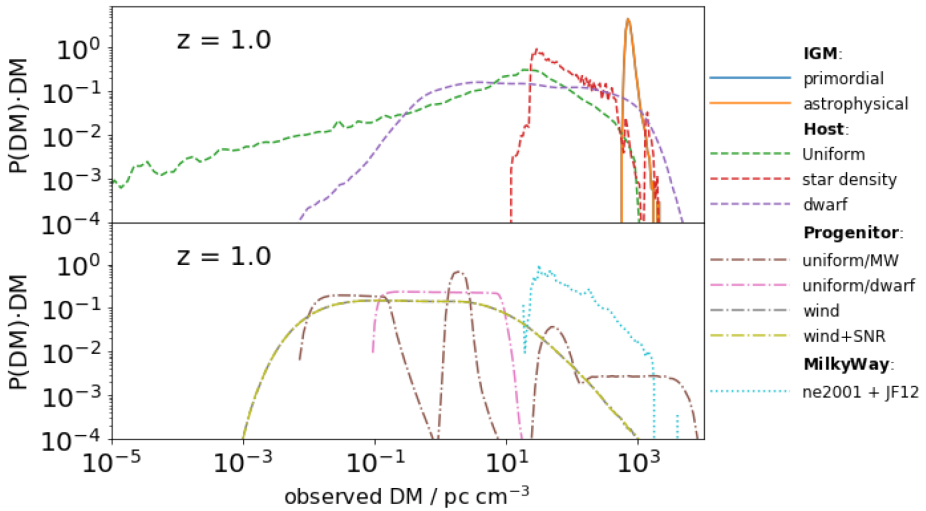


Figure 9. Likelihood functions $P(\text{DM}|z=1)$ for all contributor models investigated in this work. The linestyle indicates the contributing region described by the model.

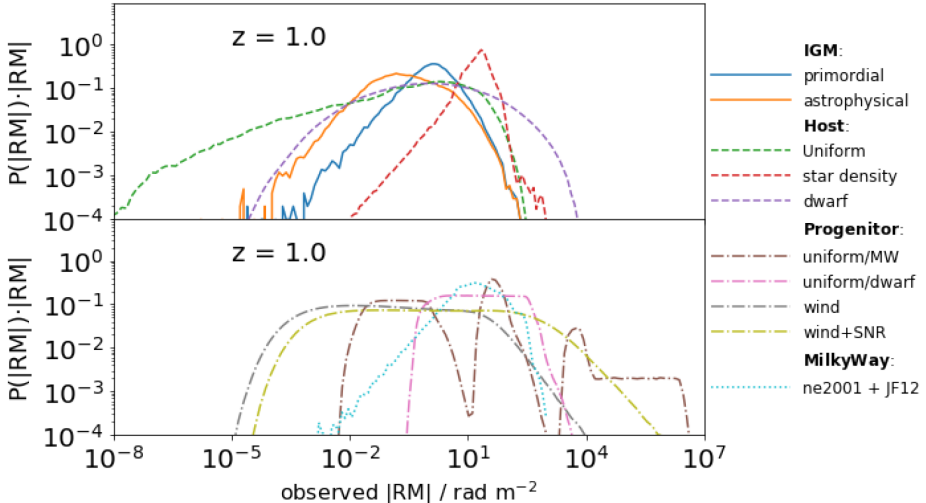


Figure 10. Likelihood functions $P(\text{RM}|z=1)$ for all contributor models investigated in this work. The linestyle indicates the contributing region described by the model.

density. This falls off exponentially with distance from the centre of the galaxy, which hosts most candidate locations and gives the strongest contribution to RM_{host} .

For a *Uniform* distribution of progenitors, there is a wide and pronounced tail towards lower values of RM_{host} , due to the numerous short LoSs of progenitors located at the border of the galaxy. In this case, the bulk of RM_{host} is comparable to the IGM contribution. These models are in best agreement with the results by Basu et al. (2018), who investigated the RM contribution of a randomly orientated galaxy in the LoS of a quasar. The range up to \lesssim few 100 rad m^{-2} and median $\approx 10 \text{ rad m}^{-2}$ of their distribution is comparable to our results.

The starburst *dwarf* galaxy model assumes the distribution of progenitor positions to be concentrated close to the galactic centre. Overall, the contribution is stronger than for a *Uniform* distribution of sources in a spiral galaxy, since most LoSs traverse considerable portions of high-density regions in the galactic disc. Due to the small size of a dwarf galaxy, the majority of LoSs show RM_{host}

below the most probable value found for *star density* distribution in spiral galaxies.

The *uniform* model of the local environment of neutron stars described in Piro & Gaensler (2018) strongly depends on the local ISM density n_{ISM} . Hence, the shape of the likelihood function is determined by the prior distribution chosen for n_{ISM} and allows us to easily associate RM_{prog} with the medium around the progenitor. This depends on the galaxy that hosts the FRB and we present results for both models of the host galaxy investigated in this work. In case of a spiral galaxy like the MW, we see that for magnetars located in H II regions, the contribution of the remnants of the recent supernova can reach extremely high RM_{prog} up to several 10^6 rad m^{-2} , exceeding RMs in that region observed with background sources by several orders of magnitude (e.g. Harvey-Smith, Madsen & Gaensler 2011).

There is a reasonable probability of about 1 per cent to see $\text{RM}_{\text{prog}} \gtrsim 10^4\text{--}10^5 \text{ rad m}^{-2}$ from magnetars in these regions. This suggests that the high RM_{obs} of FRB121102 (Michilli et al. 2018) might be the signal of an FRB located in an H II region. However, the bulk of

RM_{prog} expected in both models is of the order of the contribution of the IGM or the MW.

If the local environment of the magnetar was instead dominated by the stellar *wind* of the seed star, the likelihood function of RM_{prog} is rather flat (10^{-4})–(10^1) rad m^{-2} with rapidly falling tails on both sides. Adding the SNR contribution in *wind*+SNR, the plateau expands to 10^3 rad m^{-2} with a high-end tail reaching out to 10^5 rad m^{-2} . However, it barely reaches values high enough to explain the high RM_{obs} of FRB121102. Since this model is more of an upper limit than a prediction, this scenario is highly unlikely. Therefore, the best-fitting scenario for FRB121102 from the models of this paper is a magnetar localized in an H II region. This is in close agreement with previous works, which concluded that FRB121102 is likely produced by a magnetar in high-density regions (Masui et al. 2015; Spitler et al. 2016; Beloborodov 2017). Note, however, that a wide range of sizes and densities of H II regions is excluded by constraints from DM and the absence of free–free absorption (Michilli et al. 2018).

3.4 Dependence on redshift

From the likelihood functions derived above, we compute the expectation value and deviation of the contributor models in order to compare their contribution at different redshifts more easily. The results are shown in Fig. 11.

The MHD simulations probed by Vazza et al. (2018) are produced in the same framework. We use similar starting parameters, adding the constrained initial conditions. The resulting LoSs are, statistically speaking, almost identical. The redshift dependence of the average $\langle \text{DM} \rangle$ contribution of the IGM compares well to the results of Akahori et al. (2016). Since the other extragalactic contributions decrease with redshift, the IGM strongly dominates the total DM_{obs} at redshifts $z \gtrsim 1$. However, there is little change in DM_{IGM} with redshift $z > 1$ –2. This introduces huge uncertainties in estimating the corresponding redshift for high DMs.

At low redshifts, $z < 0.1$, the IGM contribution is substantially subdominant to the contributions of the MW and the host galaxy. Hence, the DM_{obs} can only provide an upper limit on z (cf. Dolag et al. 2015; Niino 2018; Walker et al. 2018; Pol et al. 2019). The different models for progenitor environment and host galaxy do not show significant differences.

For the $\langle \text{RM} \rangle$, the different models of progenitor environment and host galaxy result in rather different contributions. For example, a spiral galaxy similar to the MW on average contributes two orders of magnitude higher RM_{host} than a dwarf galaxy similar to IC 10.

Regardless of the model, the contribution from the host galaxy and/or the progenitor environment dominates the RM_{obs} of FRBs in the local Universe $z < 0.1$. The choice of models determines at which point the IGM will take over. Although the contribution of the MW is dominant at all redshifts up to $z = 6$, we argue that this contribution can be removed by subtracting the MW component with sophisticated modelling of the Galaxy (Boulanger et al. 2018). At high latitudes, $\text{RM}_{\text{MW}} \approx 10 \text{ rad m}^{-2}$ are still very likely. Hence, it does not suffice to restrict the sample to FRBs observed outside the Galactic plane.

The difference in average $\langle \text{RM}_{\text{IGM}} \rangle$ between the primordial and astrophysical models is about one order of magnitude at $z = 1$. That difference increases with redshift to almost two orders of magnitude at $z = 6$, where the *primordial* model is dominant over all other extragalactic contributions. This shows that RM_{EG} of FRBs delivers information on and can be used to constrain the strength and origin of the IGMF. However, the minimum redshift of FRBs required to

allow us to derive conclusions strongly differs for different host galaxies and progenitor environments.

4 COMBINED RESULTS

4.1 Extragalactic likelihood function

In the previous sections, we derived likelihood functions for all extragalactic contributors of DM_{obs} and RM_{obs} measured for FRBs. In this section, we combine these results into a likelihood function for the total extragalactic contribution. The combined likelihood function of the sum of independent variables is the convolution of their individual likelihood functions,

$$P_{\text{EG}} = P_{\text{IGM}} * P_{\text{host}} * P_{\text{prog}} \quad (7)$$

We stress that the results presented in this section cannot yet be compared to observations directly, without assumptions on the FRB population and observational selection effects. If, for example, the number of FRBs increases with redshift, higher values of DM and RM are expected than for a constant number of FRBs. In the future, population assumptions and selection effects will be implemented using results of FRBPOPPY¹ in order to provide detailed predictions, tailored to the individual telescope, to be compared to observations.

We compute the likelihood of the extragalactic component DM_{EG} , assuming that FRBs are produced in a *wind* progenitor environment hosted by a starburst *dwarf* galaxy. This set of models was chosen in order to obtain the most optimistic results on obtaining info about the IGMF. Since the density distribution is the same in the *primordial* and *astrophysical* IGM models, we only show results for the former. These are shown in Fig. 12 for FRBs at different redshifts.

As explained in the previous section, the DM_{EG} is strongly dominated by the IGM at high redshifts $z > 1$. Therefore, the combined likelihood function is almost identical to that of the IGM alone. The distribution in Fig. 12 becomes much narrower. The range reduces from over two orders of magnitude, $\sim 10^2$ – 10^4 pc cm^{-3} , at redshift $z = 0.1$ to a range of less than factor 2 at redshift $z = 6$, peaked at around $2 \times 10^3 \text{ pc cm}^{-3}$. The peak value is determined by the IGM and increases with redshift. The tail to high RM_{EG} , provided by strong progenitor contribution, decreases and is completely overshadowed by the IGM distribution by redshift $z \approx 1$. However, the increase of the peak value is rather slow at high redshift. This introduces a high uncertainty in determination of the exact redshift using DM_{obs} .

The contribution of the host galaxy can cause huge values of observed DM_{host} , which exceed the contribution of the IGM even at very high redshifts, $z \gtrsim 6$. Therefore, high DMs do not necessarily imply a high redshift of the source, but could also be produced in a nearby host galaxy. Note, though, that the likelihood of high DM_{host} at low $z < 1$ is rather low, \lesssim few per cent, as the bulk of DM_{host} is about an order of magnitude below results of the IGM at $z > 1$. If the observed amount of FRBs with high DMs is found to be $\gtrsim 5$ per cent, this would allow us to conclude on a cosmic population $z > 1$.

We further compute the likelihood of the extragalactic component RM_{EG} , assuming that FRBs are produced in a *wind* progenitor environment hosted by a starburst dwarf galaxy. To see the difference for the scenarios of magneto-genesis of IGMFs, we compute results for

¹<https://github.com/davidgardenier/frbpoppo>

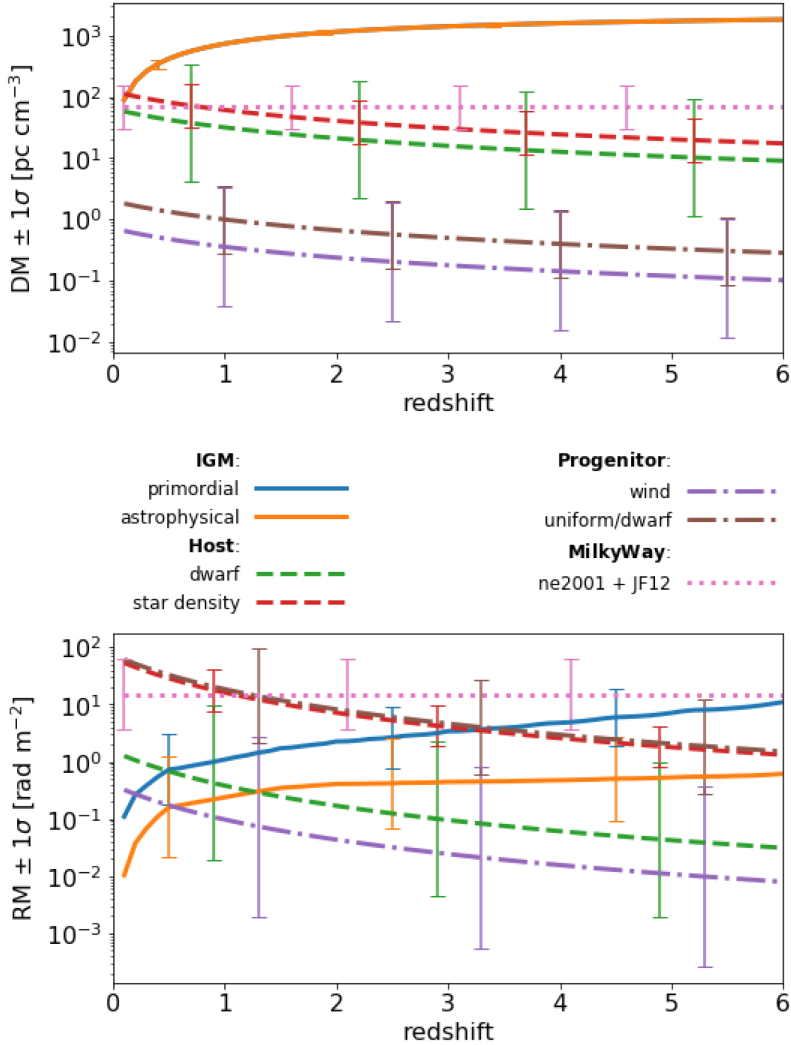


Figure 11. Redshift dependence in the distant Universe of the different average contributions $\langle \text{DM} \rangle$ (top) and $\langle \text{RM} \rangle$ (bottom).

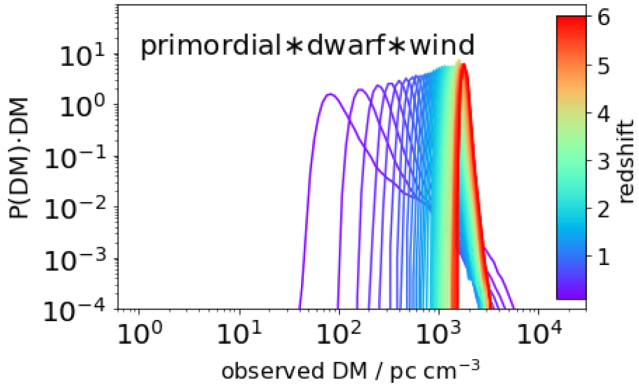


Figure 12. Combined likelihood function P_{DM} of all extragalactic contributors to DM, assuming that FRBs are produced at redshift z in a *wind* progenitor environment and hosted by a starburst *dwarf* galaxy embedded in an IGMF of *primordial* origin. From blue to red, the graphs show results for increasing redshift in the distant Universe, $0.1 \leq z \leq 6.0$ in steps of 0.1.

both the *primordial* and *astrophysical* cases. The results for FRBs at different redshifts are shown in Figs 13 and 14.

At low redshift, the shape of $P(\text{RM}_{\text{EG}}|z)$ is determined by the host contribution. However, there is a significant difference between the two models, already at $z = 0.5$, that grows with redshift, though the average of both distributions is comparable. A quantification of that difference can be found in Section 4.2.

For the *primordial* model, contributions from the IGM become comparable to the host contribution at $z \approx 0.5$. This allows us to lower the chance of the highest RM_{EG} due to cancellation of RM from different regions, while intermediate results $\gtrsim 1 \text{ rad m}^{-2}$ become more likely.

At higher redshift, $z \gtrsim 4$, the shape is completely determined by the IGM contribution, as it exceeds the observed contribution of the host galaxy at such high redshifts. This shows the capability of RM_{obs} of FRBs to shed light on the origin of IGMFs.

Note that, although the values of RM_{IGM} in the *astrophysical* case are equal or smaller than in the *primordial* case, there can be a slightly higher chance of a high RM_{EG} in the former case. This is because RMs from different regions of the LoS, e.g. IGM and host, can cancel each other. Hence, two comparably strong contributors

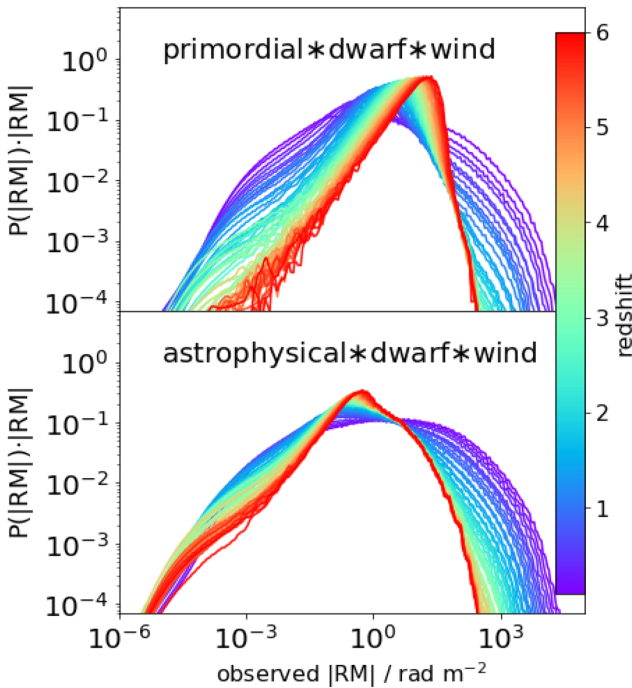


Figure 13. Combined likelihood P_{EG} of all extragalactic contributors to RM, assuming that FRBs are produced at redshift z in a *wind* progenitor environment and hosted by a starburst *dwarf* galaxy embedded in an intragalactic magnetic field of *primordial* (top) or *astrophysical* (bottom) origin. From blue to red, the graphs show results for increasing redshift in the distant Universe, $0.1 \leq z \leq 6.0$ in steps of 0.1.

can weaken the likelihood for high RM_{obs} , as compared to only one dominant contributor. Use of the likelihood function can account for that, which is an advantage as compared to considering only the average value.

We stress that results in this section highly depend on the choice of contributor models. Here, we made use of those host galaxy and progenitor environment models, which showed the least contribution to RM_{EG} . We did this in order to derive the most optimistic results on obtaining info on the IGM. The results in Figs 9–11 show that the other host and progenitor models investigated here provide much higher values of RM that overshadow the IGM contribution up to redshift $z = 3\text{--}4$. Ways to restrict the inference to those FRBs that fit the presented choice of models will be discussed in Section 5 and will be the subject of upcoming works.

4.2 Application to observations

At this point, there are few observations of FRBs with RM_{obs} . This will change soon, after new telescopes dedicated to observe FRBs, e.g. CHIME/FRB, FAST, SKA, and MeerKat, begin producing RM data (Jonas 2009; Nan et al. 2011; Keane et al. 2013; Macquart et al. 2015; The CHIME/FRB Collaboration 2018). We therefore investigate samples of random tuples of DM and RM that resemble the expected distribution at redshift $z = 0.5$ shown in Figs 7 and 14. Note that contributions from the ionosphere to the RM are expected to be a few rad m^{-2} (Weisberg et al. 2003), therefore hampers investigation of the distribution of $\text{RM}_{\text{obs}} < 1 \text{ rad m}^{-2}$. To account for that, we only sample RM above that value.

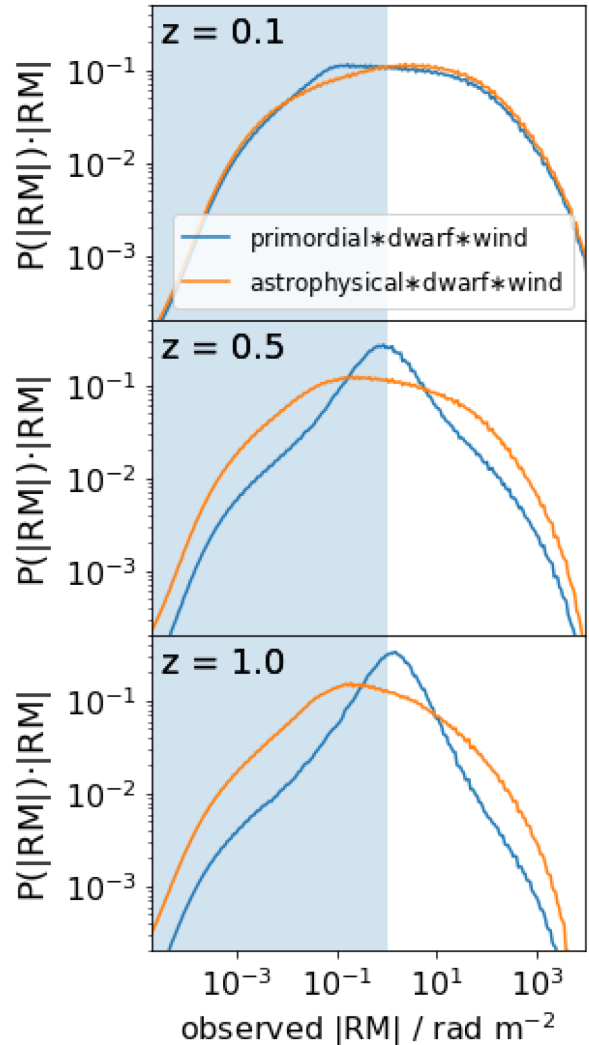


Figure 14. Same as Fig. 13 with both models in a single plot for a small set of redshifts to allow better comparison. The grey area indicates $\text{RM}_{\text{EG}} < 1 \text{ rad m}^{-2}$ that we consider as not observable due to uncertainties in removing the foreground of the MW and ionosphere.

For each of the (DM, RM) tuples, we compute the Bayes factor $b(\text{DM}, \text{RM}|\text{primordial}, \text{astrophysical})$

$$= \frac{P(\text{DM}, \text{RM}|\text{primordial})}{P(\text{DM}, \text{RM}|\text{astrophysical})}, \quad (8)$$

which quantifies how much more likely it is that the given tuple of DM_{EG} and RM_{EG} is produced in the *primordial* rather than in the *astrophysical* case. A Bayes factor $b(O, M_1, M_2) > 10$ shows that observation O is more than 10 times more likely in model M_1 than in model M_2 . This signals strong evidence in favour of M_1 as compared to M_2 . For values $b > 100$, the evidence is considered to be decisive (Jeffreys & Jeffreys 1961).

The likelihood of two events is the product of their individual likelihoods. The same holds for the Bayes factor, which applies a number to our corroboration towards one model over the other.

In particular, we use the DM_{EG} to derive a likelihood function $P(z|\text{DM}_{\text{EG}})$ for the redshift of the FRB. This is then used as a prior

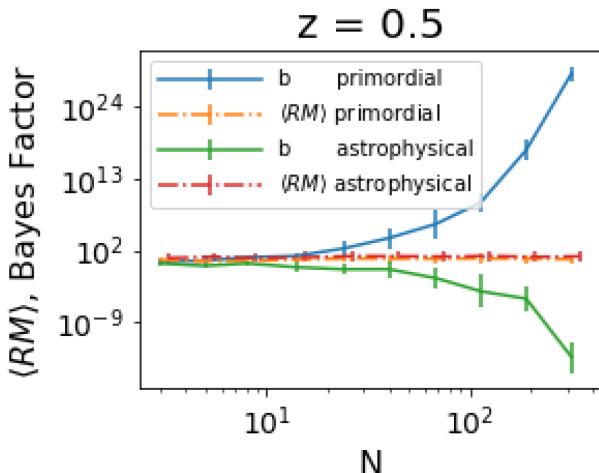


Figure 15. Bayes factor b and average $\langle \text{RM}_{\text{EG}} \rangle$ for two fake populations at the indicated redshift that resemble the *primordial* and *astrophysical* cases. The errorbars of $\langle \text{RM}_{\text{EG}} \rangle$ show the 1σ standard deviation of RM in the population. For b , they show the standard deviation of six random samples of the population.

to derive the likelihood of the RM_{EG}

$$P(\text{DM}_{\text{EG}}, \text{RM}_{\text{EG}} | BO) \propto \int P(\text{RM}_{\text{EG}} | BO, z) P(z | \text{DM}_{\text{EG}}) dz. \quad (9)$$

Note that this inference does not require knowledge on the redshift of the FRB, but only uses the DM_{EG} and RM_{EG} . If the redshift is known, $P(z | \text{DM}_{\text{EG}})$ can be replaced by a narrower function in order to decrease the range of possible RM_{EG} in the different models and allow for more precise results.

Note that RMs from AGNs are much easier to be associated with a redshift. Hence, including AGNs in our analysis in future work will significantly improve the results of this section, despite the missing DM.

We compute the Bayes factor for different sizes of the sample to see how many FRBs are required at a given redshift in order to allow conclusions on the IGM. We also compute the average $\langle \text{RM}_{\text{EG}} \rangle$ of these samples to compare the efficiency of the Bayesian inference to the frequentists' approach. The results are shown in Fig. 15.

The $\langle \text{RM}_{\text{EG}} \rangle$ agree within 1σ standard deviation for both populations, whereas the Bayes factor shows a difference $\gtrsim 10$ orders of magnitude for a number of 100 FRBs at redshift $z = 0.5$, in case they are produced by magnetars in wind environments hosted by dwarf galaxies. This huge difference clearly sets apart the scenarios for the generation of the IGMF.

We stress that this result is largely dependent on the assumed model for the host galaxy and progenitor environment since Fig. 11 shows that other choices lead to very different results. This can shift the required redshift of FRBs, e.g. hosted by spiral galaxies, to much higher redshifts, $z \gtrsim 3$ or even above. Hence, an identification of the host galaxy as well as the local environment of the progenitor is crucial for their use to probe IGMFs. This can be a difficult task, especially for the case of dwarf galaxies (e.g. Eftekhari & Berger 2017).

We compare several possible combinations of models to investigate the redshift of FRB sources required to obtain information on the IGMF in those scenarios. We sample DM_{EG} and RM_{EG} of 100 FRBs, all at the same redshift and compute the corresponding Bayes factor $b(\text{DM}, \text{RM} | \text{primordial, astrophysical})$ (equation 8). This procedure is then repeated with increasing redshift. We

compute six random samples at each of these redshifts and plot the average and standard deviation of the Bayes factor. The results are shown in Fig. 16.

For three of the seven combinations of models, at redshifts $z \lesssim 0.5$, the resulting Bayes factor is $b \gg 10^2$ and hence clearly speaks for a *primordial* origin of IGMFs (in case of a *primordial* fake population). The same holds for the *astrophysical* scenario. These are the combinations that assume the *wind* or *wind+SNR* model for the progenitor together with a *dwarf* host galaxy. The *wind* model delivers a distribution of RM_{prog} that is more concentrated on lower values as compared to the *uniform* model. Though the former delivers much higher values of RM_{prog} , this is mostly for times $t \lesssim 25$ yr, below which the radio bursts are weakened by the supernova ejecta (Margalit et al. 2018). At later times, the predicted RM_{prog} decreases much faster in the *wind* than in the *uniform* case, accounting for the higher amount of low RM_{prog} in the former case.

The third combination considers both galaxy models, the *dwarf* as well as the MW-like spiral galaxy, *star density*, as equally likely hosts. This is done by using the renormalized sum of both likelihood functions, shown in Figs 9 and 10. The resulting distribution is much less peaked than the *star density* case and tends to lower values, therefore enabling those FRBs to deliver information on the IGM. This means that, even if not all of the FRBs taken into account are hosted by *dwarf* galaxies, their overall statistics at redshift $z \gtrsim 0.5$ may still allow us to draw conclusions on the magneto-genesis of IGMFs.

We note that the equal weighting of the two host models is an arbitrary choice, not based on any realistic population synthesis of galaxies. In reality, the weighting for different types of galaxies changes with redshift, as does the galactic stellar mass function (e.g. Lilly et al. 2009) as well as the major star population and their age in different types of galaxies (e.g. Hopkins 2004). An increase of the weight of spiral galaxies, *star density*, would increase probability of strong host contributions and hence push the redshift required to probe the IGM to higher values. Future work should account for that by assuming several possible populations of FRBs, their possible host galaxies and redshift distribution.

Four of the seven combinations result in indecisive Bayes factors, $b \lesssim 10^2$, at redshifts below $z \lesssim 3$. These are scenarios that assume either an MW-like galaxy, *star density*, as the host of FRBs with any model for the progenitor investigated in this work, or a magnetar embedded in a *uniform* environment hosted by a *dwarf* galaxy. In these cases, the local contribution is too strong to allow us to infer information on the IGM. For the spiral galaxy model, the distribution of RM_{host} peaks at about $\gtrsim 10^1$ rad m $^{-2}$ in the host rest frame. This strong contribution can overshadow the contribution from the IGM at high redshift. However, even for these unfavourable models, beyond redshifts of $z \gtrsim 3.5$ –4, the contribution of the IGM becomes strong enough to allow to distinguish between different scenarios of magneto-genesis of IGMFs. FRBs at such high redshift probably will not even require us to select a special subset of the population, e.g. hosted by dwarf galaxies, in order to obtain reasonable results. However, using only FRBs beyond redshift $z \sim 4$ might be even harder to accomplish, as it is a tough task, in case they exist, to find the exact redshift of FRBs at this distance. On the one hand, the DM can only be used to derive an upper limit on z , as we show in Section 4. On the other hand, identification of the a dwarf host galaxy becomes increasingly harder with growing redshift (e.g. Eftekhari & Berger 2017).

Note that the *dwarf*uniform* case shows vastly lower values of the Bayes factor at redshifts $z > 4$ than all of the *star density* combinations. The latter are dominated by the host contribution

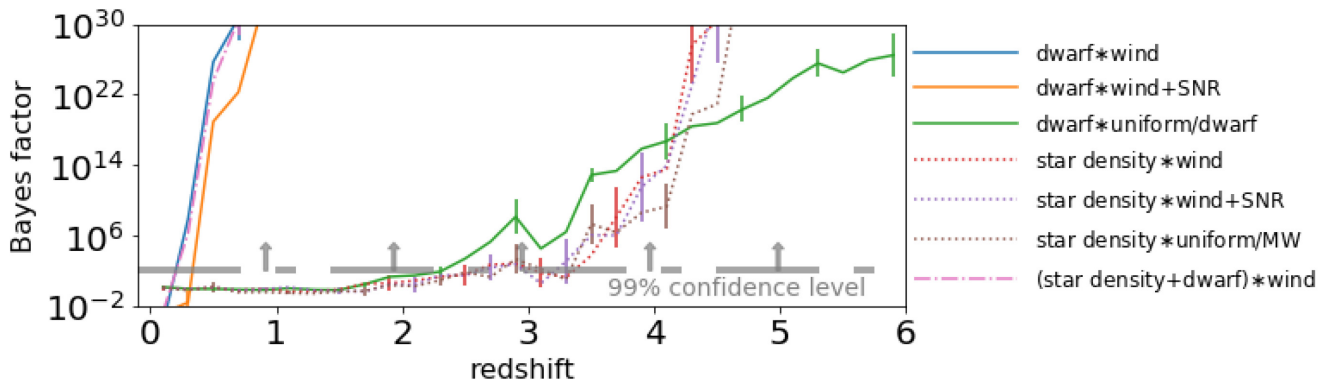


Figure 16. Bayes factor for fake samples of 100 FRBs at different redshifts, resembling the population in the *primordial* magneto-genesis scenario, combined with several sets of models indicated by colours and linestyles. The solid lines consider a *dwarf* galaxy as the host of FRBs, the dotted lines assume the MW-like spiral galaxy, *star density*, while the dash-dotted line allows for both of these galaxy types to host similar numbers of FRBs. The grey line marks a Bayes factor of 10^2 , which indicates a 100 times higher chance for the fake population to be produced in the *primordial* rather than in the *astrophysical* scenario, assuming the same models for the other contributors. This indicates the 99 per cent confidence level to rule out the latter scenario in favour of the former.

for all models of the progenitor environment. The very narrow distribution $P(\text{RM}_{\text{host}}|\text{star density})$ peaks between the *primordial* and *astrophysical* $P(\text{RM}_{\text{IGM}})$. Their convolution, $P_{\text{Host}} * P_{\text{IGM}}$, is rather different for the two cases.

In contrast, the *dwarf*uniform* case is dominated by the local environment of the progenitor, which shows a very flat distribution, $P(\text{RM}_{\text{prog}})$, due to the assumed flat prior. The *primordial* $P(\text{RM}_{\text{IGM}})$ peaks within the range of $P(\text{RM}_{\text{prog}})$; their convolution, $P(\text{RM}_{\text{EG}})$, has similar shape to $P(\text{RM}_{\text{prog}})$, altered only by a subtle peak at high values. The primarily low contributions of the *astrophysical* RM_{IGM} do not alter the shape of $P(\text{RM}_{\text{prog}})$ significantly. Hence, the full likelihood functions $P(\text{RM}_{\text{EG}})$ have similar shape for both models of the IGM. Single events have less weight as evidence because the Bayes factor is generally closer to unity. In mathematical terms, the integral over the absolute difference of the likelihood functions of the two cases is higher for the *star density* galaxy combinations than for the *dwarf*uniform* case, which is hence less informative. Note that this is another measure that might be used to infer the likelihood of different combinations of models.

Note further that for all four of these models, the Bayes factor b drops significantly at around $z \approx 3$. This is because the shapes of $P(\text{RM}_{\text{host}}|\text{star density})$ and $P(\text{RM}_{\text{IGM}}|\text{primordial})$ are almost identical, as their peaks move through the same value at this redshift. This causes the two contributions to greatly match each other, resulting in an identical shape of the full $P(\text{RM}_{\text{EG}})$. In contrast to that, RM_{IGM} values in the *astrophysical* scenario are too weak to significantly alter the shape of $P(\text{RM}_{\text{host}})$. Hence, the two IGM scenarios appear very similar at that redshift. This cosmic conspiracy might be used to infer the strength of the primordial magnetic field B , as the position of the dip highly depends on B . However, it also strongly depends on the shape of the contribution of the host galaxy and might not be visible for other sets of models.

We have shown that there likely exists at least a subset of FRBs – produced by magnetars in wind environments hosted by starburst dwarf galaxies – that carries information on the IGMF. However, other host galaxies and progenitor classes completely overshadow that signal of the IGM. This shows how important it is to carefully consider the numerous possible models for regions along the LoS and to identify the host galaxies and source objects in order to measure the IGMF using FRBs.

According to the Bayes' theorem, in order to arrive at the ratio of posterior likelihoods L for the different models, the Bayes

factor B has to be multiplied by the prior corroboration $\pi(M)$ towards a model M , based on information other than the investigated observation O (e.g. Boulanger et al. 2018; Fraix-Burnet et al. 2018):

$$\frac{L(M_1|O)}{L(M_2|P)} = b(O|M_1, M_2) \times \frac{\pi(M_1)}{\pi(M_2)}. \quad (10)$$

Note that we assume the two IGM models to be equally likely, i.e. $\pi = \text{const}$. It therefore suffices to investigate the Bayes factor b to infer the posterior likelihood of different models.

5 DISCUSSION

We investigate whether observations of FRBs can deliver information about the IGMF and its origins. To this end, we consider two extreme scenarios of magneto-genesis: a scenario where the IGMF is seeded at very high redshift (termed *primordial* scenario) and a second scenario where the magnetic field is mainly supplied by galactic outflows and other astrophysical processes (termed *astrophysical* scenario).

The initial magnetic field is very different in the two scenarios. Hence, the two scenarios account for a strong difference in the strength of magnetic fields far outside the overdense regions in the Universe. This implies significantly different results for the RM and makes these two suitable models to investigate the potential of FRBs to probe the IGMF. We compute likelihood functions of these measures that allow a comparison of the assumed models to observational data.

To account for the contribution towards the rotation and dispersion measures of the host, we investigated two models for the host galaxy, i.e. an MW-like spiral galaxy and a starburst dwarf galaxy similar to IC 10 or the host of FRB121102. This only serves as an illustration of our framework to compare theory and observations and this framework can easily be expanded to include a large variety of models for the host galaxy. Results agree with previous works (Xu & Han 2015; Basu et al. 2018).

Likewise, we model in Section 2.3 the contribution of the local environment of the progenitor with Monte Carlo simulations using the results of Piro & Gaensler (2018). The source of FRBs is assumed to be a magnetar embedded either in a uniform ISM or an environment disturbed by stellar winds of the seed star. For the *uniform* case, the distribution of possible ISM number densities n_{ISM} is determined by the host galaxy.

In accordance with previous work (Dolag et al. 2015; Niino 2018; Walker et al. 2018; Pol et al. 2019), we find that the DM is an imprecise measure of the source redshift and only delivers reasonable upper limits. Only few of the investigated models had low probability to supply DM in excess of DM_{IGM} . Hence, a significant fraction $\gtrsim 5$ per cent of high $\text{DM}_{\text{obs}} \gtrsim 10^3 \text{ pc cm}^{-3}$ would point to a population of FRBs at cosmic distance, $z \gtrsim 1$. However, this requires a more detailed investigation that takes into account the uncertain evolution of the number of FRB sources with redshift, as well as the selection effects of the telescopes. We note that this is the scope of FRBPOPPY!² the results of which will be implemented in this framework in the future.

Bhandari et al. (2017) report three FRBs with very high $\text{DM}_{\text{obs}} > 1500 \text{ pc cm}^{-3}$ detected by the Parkes telescope. Although the DMs are highly debated to be produced locally, they raise hope that there is indeed an FRB population at large distance that will be detected in the years to come. For example, the MeerKat and Parkes telescopes can detect FRBs out to redshift $z \approx 4$ (Keane 2018). Arecibo may detect bursts at $z \approx 5$ (Lorimer 2018), while FAST will be able to detect FRBs even out to $z \approx 15$ (Zhang 2018), with DM_{obs} exceeding 10^4 pc cm^{-3} . Our study shows that these FRBs are an interesting source of information on the IGMF and its origins.

For the limited set of models investigated in this paper, only a few progenitor models are capable to produce the high RM observed for FRB121102 (Michilli et al. 2018). For other FRBs with less extreme RMs, conclusions on their source are less obvious and require careful investigation of the convolved likelihood functions of the different contributors. The time evolution of repeating FRBs can be used to put much better constraints on the source model. This is, however, beyond the scope of this study and will be considered in upcoming work.

The models applied for the host galaxy use analytic functions and do not account for local overdensities, which can add significantly to RM_{host} . Also, our models of the host do not yet account for cosmic evolution of the galaxy. Results of Pillepich et al. (2019) suggest that low-mass star-forming galaxies do not change their size significantly out to redshift $z = 4\text{--}5$. Hence, the values of DM_{host} are not expected to change much for the dwarf-type of galaxies considered here. They further find that massive galaxies similar to the MW tend to be smaller at higher redshift. The density can be higher by a factor of few tens, while the path-length is reduced by a factor of a few, accounting for a DM higher by about one order of magnitude than predicted in our model, still mostly below the contribution of the IGM.

For magnetic fields in galaxies, the amplification time is of the order of $10^7\text{--}10^8$ yr (e.g. Schober, Schleicher & Klessen 2013). Observations and simulations of galaxies at high redshift suggest magnetic fields of similar strength as in present-day galaxies (Bernet et al. 2008; Kronberg et al. 2008; Pakmor, Marinacci & Springel 2014; Mao et al. 2017). Hence, the expected change to the RM_{host} is of the same order as for the DM_{host} , insignificant for dwarf-type and about one order of magnitude higher for galaxies similar to the MW. This implies that the latter type of host dominates the extragalactic contribution and does not allow for conclusions on the IGMF, even out to redshift $z = 6$. However, Rodrigues et al. (2018) conclude that a significant fraction of massive spiral galaxies contain negligible large-scale magnetic fields at redshifts $z > 3$, suggesting a significantly weaker host contribution. A more physical modelling of the host galaxies will be the subject of future work.

²<https://github.com/davidgardenier/frbpoppo>

We account for effects from the possible progenitor positions by testing different distributions within the host galaxy. We find that assuming a uniform distribution in the host disc affects the distribution of expected DM_{host} only at values $\lesssim \text{few pc cm}^{-3}$, as compared to a distribution that concentrates on the centre of the galaxy.

The distribution of expected RM_{host} is very different, even $\gtrsim 10^1 \text{ rad m}^{-2}$, close to the maximum possible value, with a much higher probability in the centred case because the highest RM_{host} come from the centre of the galaxy. We note, however, that our model does not include the high $\text{RM} \approx -5.6 \times 10^5 \text{ rad m}^{-2}$ found for Sagittarius A* (Marrone et al. 2006). Such contributions from a LoS through the galactic centre of the host galaxy might explain the high RM observed for FRB121102 (Michilli et al. 2018). We argue that such LoSs are very unlikely for progenitors that are not themselves located in the centres of their host galaxy.

By assuming only magnetars as progenitors, we restrict the parameter space for equations in Piro & Gaensler (2018), as compared to neutron stars with weaker magnetic fields, e.g. pulsars. By that, we mostly exclude lower values of RM_{prog} , hence arrive at rather optimistic predictions for the contribution from the local environment of the progenitor. Further, their model assumes that shocks in supernova remnants produce coherent magnetic fields, while it most likely has a random topology. Hence, the results for the *uniform* and the *wind+SNR* model should be considered as upper limits. In case the real contribution of RM from such magnetars is significantly lower, these sources might also deliver information on the IGMF.

We do not account for the contributions of the MW halo. For the DM, they are comparable to the contribution from the Galactic disc, $\approx 30\text{--}80 \text{ pc cm}^{-3}$ (Dolag et al. 2015; Prochaska & Zheng 2019). The RM from the halo is probably lower than from the disc, due to the weaker magnetic fields. However, the likelihood function of the two models for the IGM show reasonable difference at redshift $z = 0.5$ even for $\text{RM}_{\text{EG}} > 1 \text{ rad m}^{-2}$. We only used RM_{EG} above this value in estimates of the model likelihood in Section 4.2.

We do not account for the distribution of galaxies that host FRBs. By applying a constant weight to each LoS, we implicitly assume a uniform distribution of host galaxies. Reducing the weight of LoS through low-density regions mostly reduces the likelihood of low values of RM that cannot be probed by telescopes. Estimating the effect on likelihood of $\text{RM} \gtrsim 1 \text{ rad m}^{-2}$ is not trivial and will be studied in upcoming works. However, for FRBs beyond redshift $z \gtrsim 0.1$, the overall statistics are not expected to change, since the Universe is homogeneous on large scales.

We do not account for the contribution of intervening galaxies (e.g. Basu et al. 2018). If the intervening galaxy is of the same type as the host, the contribution is comparable to the host contribution at the redshift of intersection and therefore hampers the investigation of the IGM component (Zheng et al. 2014). If the pulse broadening of FRB radiation is found to be dominated by scattering in intervening galaxies, this can help to exclude LoS with a significant contribution of intervening galaxies (Lorimer et al. 2013; Spitler et al. 2014). This will be a subject of future studies.

Our results are provided in the form of likelihood functions for the different contributions to RM and DM. We show how these likelihood functions can be used for parameter inference. This framework can help to infer the origin of FRBs as well as the origin of extragalactic magnetic fields (Caleb et al. 2018; Katz 2018; Palaniswamy et al. 2018).

6 CONCLUSIONS

In this paper, we have studied the different contributions to the DMs and RMs along the lines of sight of FRBs. We have built a Bayesian framework to interpret observable information of FRBs. We show how this can be used to constrain the amplitude of magnetic fields in the IGM along the line of sight. Our key findings are as follows:

(i) The strengths of the different contributions to the observed RM_{obs} highly depend on the assumed model for FRBs and their host galaxies. Magnetars embedded in wind environments hosted by starburst dwarf galaxies provide the lowest average local contribution to RM of the investigated models. For this generous set of models, RM_{EG} from redshifts $z \gtrsim 0.5$ can potentially provide information on the magnetic field in the IGM and its origin. At this redshift, the contribution of the IGM is still subdominant to that of the host. Still, there is a significant change in the distribution of extragalactic RM_{EG}. This allows one to draw conclusions on the magnetic field using Bayesian inference.

Conversely, for other models of the host galaxy and progenitor, the expected local contribution can be significantly stronger. These models require FRBs beyond $z \gtrsim 3$ in order to probe IGMFs. We conclude that there are good reasons to believe that at least a subset of FRBs observed with RMs delivers information on the IGMF and its origin. How to identify this subset will be subject of future studies.

(ii) The MW provides the dominant contribution of RM, even for FRBs out to redshift $z \gtrsim 6$. A prerequisite for the above result is the removal of the contribution of the MW to a precision of $\sim 1 \text{ rad m}^{-2}$. This is non-trivial, as argued by Han (2017), who suggested that up to $\sim 10^4\text{--}10^5$ values of RM may be necessary to tell apart Galactic from extragalactic contributions. However, the fast growing level of complexity in modelling magnetic fields in the MW is expected to improve at the same pace as RM statistics, making the removal of the MW foreground more viable (for a recent review, see e.g. Boulanger et al. 2018).

(iii) Using likelihood functions allows one to infer information on the host galaxy and progenitor. They allow us to systematically rule out models for a single FRB or groups of those.

(iv) From the present set of models, only some progenitor models are capable of producing the very high RM_{obs} of FRB121102. Our results suggest that, if the progenitor is a magnetar, then it is most likely located in a dense environment, such as an H II region, which we found to be capable of producing RMs that exceed those of FRB121102 by two orders of magnitude. Note, however, that the strong magnetic fields generated by shocks in the supernova remnants are likely random. This can result in much lower RM than predicted by the model of Piro & Gaensler (2018), who assumed a coherent magnetic field.

We find a much smaller chance that stellar winds of the seed star in other environments can account for the high RM_{obs} as well. The shape of magnetic fields induced by stellar winds is very coherent and can account for very high values of RM. However, the expected RM_{prog} falls rapidly with age of the magnetar. This implies a much lower chance to observe high RM_{prog} from such a source.

We provide a framework for the comparison between observations and theories of FRBs. So far, we consider a very limited set of models in order to present our framework. Still, we could show the likely existence of a subset of FRBs that delivers information on the IGMF and its origins. Future work will include more models, such as elliptical or disc host galaxies, and take into account their evolution with redshift. We will vary the strength of a primordial

magnetic field in realistic combination with astrophysical processes. This will allow us to precisely probe the average strength of IGMFs today as well as the strength of the primordial seed field, thus allow us to constrain processes of magneto-genesis with FRBs.

At this point, we only consider the DM and RM. In future work, more observables will be considered, such as temporal scattering, flux density, and fluence. Further contributing regions will be considered, such as intervening galaxies and the halo of the MW. Combining this with knowledge on the selection effect of telescopes and assumptions on the underlying population of FRBs, we can produce individual predictions for the distribution of observables as measured at different telescopes.³

ACKNOWLEDGEMENTS

We thank Tony Piro for his help in understanding and reproducing results from his paper. We also thank Ryan Mckinven for interesting comments. Further, we thank the anonymous referee for a detailed review and constructive comments. SH would like to thank all participants of ‘A Bayesian View on the Galactic Magnetic Field’ as well as the Lorentz Center for an inspiring meeting. SH would also like to thank the organizers, speakers, and participants of the ‘Stat4Astro School of Statistics for Astrophysics 2017: Bayesian Methodology’ and the ‘FRB2019’ conference in Amsterdam for interesting discussions.

Our cosmological simulations were performed with the ENZO code (<http://enzo-project.org>), under project HHH38 and HHH42 at the Jülich Supercomputing Centre (P.I. F. Vazza). FV acknowledges financial support from the ERC Starting Grant ‘MAGCOW’, no. 714196. We thank Jenny Source and Stefan Gottlöber for providing us with the CLUES initial conditions and for their help in implementation.

The Dunlap Institute is funded through an endowment established by the David Dunlap family and the University of Toronto. BMG acknowledges the support of the Natural Sciences and Engineering Research Council of Canada (NSERC) through grant RGPIN-2015-05948, and of the Canada Research Chairs programme.

REFERENCES

- Ade P. et al., 2016, *A&A*, 594, A19
- Akahori T., Ryu D., Gaensler B. M., 2016, *ApJ*, 824, 105
- Baldry I. et al., 2012, *MNRAS*, 421, 621
- Basu A., Mao S. A., Fletcher A., Kanekar N., Shukurov A., Schnitzeler D., Vacca V., Junklewitz H., 2018, *MNRAS*, 477, 2528
- Beloborodov A. M., 2017, *ApJ*, 843, L26
- Beloborodov A. M., Li X., 2016, *ApJ*, 833, 261
- Beniamini P., Hotokezaka K., van der Horst A., Kouveliotou C., 2019, *MNRAS*, 487, 1426
- Bernet M. L., Miniati F., Lilly S. J., Kronberg P. P., Dessauges-Zavadsky M., 2008, *Nature*, 454, 302
- Bhandari S. et al., 2017, *MNRAS*, 475, 1427
- Boulanger F. et al., 2018, *J. Cosmol. Astropart. Phys.*, 2018, 049
- Bryan G. L. et al., 2014, *ApJS*, 211, 19
- Caleb M., Spitler L. G., Stappers B. W., 2018, *Nat. Astron.*, 2, 839
- Caleb M., Stappers B. W., Rajwade K., Flynn C., 2019, *MNRAS*, 484, 5500
- Campanelli L., 2009, *Int. J. Mod. Phys. D*, 18, 1395
- Chabrier G., 2003, *PASP*, 115, 763

³This is the aim of the PREFRBLB ('Predictions of FRB models and their Likelihood Estimates') python package that comes with the presented results for a fast application to observational data. This package is currently under construction and will be publicly available soon.

- Chabrier G., 2005, in Corbelli E., Palle F., eds, The Initial Mass Function 50 Years Later. Springer, Dordrecht, p. 41
- Chatterjee S. et al., 2017, *Nature*, 541, 58
- CHIME/FRB Collaboration, 2019, *Nature*, 566, 235
- Chyží K. T., Drzazga R. T., Beck R., Urbanik M., Heesen V., Bomans D. J., 2016, *ApJ*, 819, 39
- Cordes J. M., Lazio T. J. W., 2002, astro-ph/0207156
- da Silva A. C., Barbosa D., Liddle A. R., Thomas P. A., 2000, *MNRAS*, 317, 37
- de Avillez M. A., Breitschwerdt D., 2005, *A&A*, 436, 585
- Deng W., Zhang B., 2014, *ApJ*, 783, L35
- Derman E., Demircan O., Kahraman G., 1990, *A&AS*, 86, 421
- Dolag K., Gaensler B. M., Beck A. M., Beck M. C., 2015, *MNRAS*, 451, 4277
- Donnert J., Dolag K., Lesch H., Müller E., 2009, *MNRAS*, 392, 1008
- Dubois Y., Teyssier R., 2010, *A&A*, 523, A72
- Dzhatdoev T., Khalikov E., Kircheva A., Podlesnyi E., Telegina A., 2018, in Volkova V.E., Zhezher Y. V., Levkov D. G., Rubakov V. A., Matveev V. A., eds, EPJ Web Conf., Vol. 191, Intergalactic Electromagnetic Cascades in the Magnetized Universe as a Tool of Astroparticle Physics. EDP Sci. - Web Conf., Les Ulis Cedex A, France, p. 08009
- Eftekhari T., Berger E., 2017, *ApJ*, 849, 162
- Feretti L., Giovannini G., Govoni F., Murgia M., 2012, *A&AR*, 20, 54
- Ferrière K. M., 2001, *Rev. Mod. Phys.*, 73, 1031
- Fraix-Burnet D., Girard S., Arbel J., Marquette J.-B., 2018, Statistics for Astrophysics: Bayesian Methodology. EDP Sci., Les Ulis Cedex A, France, <https://hal.archives-ouvertes.fr/hal-01952759>
- Fruchter A. et al., 2006, *Nature*, 441, 463
- Górski K. M., Hivon E., Banday A. J., Wandelt B. D., Hansen F. K., Reinecke M., Bartelmann M., 2005, *ApJ*, 622, 759
- Hackstein S., Vazza F., Brüggen M., Sorce J. G., Gottlöber S., 2018, *MNRAS*, 475, 2519
- Han J. L., 2017, *ARA&A*, 55, 111
- Harvey-Smith L., Madsen G. J., Gaensler B. M., 2011, *ApJ*, 736, 83
- Heesen V., Rau U., Rupen M., Brinks E., Hunter D. A., 2011, *ApJ*, 739, L23
- Hessels J. et al., 2019, *ApJ*, 876, L23
- Hopkins A. M., 2004, *ApJ*, 615, 209
- Houben L. J. M., Spitler L. G., ter Veen S., Rachen J. P., Falcke H., Kramer M., 2019, *A&A*, 623, A42
- Hummels C. B., Smith B. D., Silvia D. W., 2017, *ApJ*, 847, 59
- Inoue S., 2004, *MNRAS*, 348, 999
- Ioka K., 2003, *ApJ*, 598, L79
- James C. W., 2019, *MNRAS*, 486, 5934
- Jansson R., Farrar G. R., 2012, *ApJ*, 757, 14
- Jeffreys H., Jeffreys H., 1961, Theory of Probability, 3rd edn. Clarendon, OUP Oxford, 1998
- Jonas J. L., 2009, *Proc. IEEE*, 97, 1522
- Jurić M. et al., 2008, *ApJ*, 673, 864
- Kahniashvili T., Tevzadze A. G., Sethi S. K., Pandey K., Ratra B., 2010, *Phys. Rev. D*, 82, 083005
- Katz J. I., 2016a, *Mod. Phys. Lett. A*, 31, 1630013
- Katz J. I., 2016b, *ApJ*, 826, 226
- Katz J. I., 2018, *Prog. Part. Nucl. Phys.*, 103, 1
- Keane E. et al., 2016, *Nature*, 530, 453
- Keane E., 2018, *Nat. Astron.*, 2, 1811
- Keane E. F., Fender R. P., Hassall T. E., 2013, *MNRAS*, 436, 371
- Kronberg P., Bernet M., Miniati F., Lilly S., Short M., Higdon D., 2008, *ApJ*, 676, 70
- Kronberg P. P., Lesch H., Hopp U., 1999, *ApJ*, 511, 56
- Kumar P., Linder E. V., 2019, preprint ([arXiv:1903.08175](https://arxiv.org/abs/1903.08175))
- Leroy A., Bolatto A., Walter F., Blitz L., 2006, *ApJ*, 643, 825
- Li B., Li L.-B., Zhang Z.-B., Geng J.-J., Song L.-M., Huang Y.-F., Yang Y.-P., 2019, preprint ([arXiv:1901.03484](https://arxiv.org/abs/1901.03484))
- Lilly S. J. et al., 2009, *ApJS*, 184, 218
- Locatelli N., Ronchi M., Ghirlanda G., Ghisellini G., 2019, *A&A*, 625, A109
- Lorimer D., Bailes M., McLaughlin M., Narkevic D., Crawford F., 2007, *Science*, 318, 777
- Lorimer D. R., 2018, *Nat. Astron.*, 2, 860
- Lorimer D. R., McLaughlin M. A., Karastergiou A., Johnston S., 2013, *MNRAS*, 436, L5
- Lu W., Kumar P., Narayan R., 2018, *MNRAS*, 483, 359
- Luo R., Lee K., Lorimer D. R., Zhang B., 2018, *MNRAS*, 481, 2320
- Lyutikov M., 2019, preprint ([arXiv:1901.03260](https://arxiv.org/abs/1901.03260))
- Macquart J. P. et al., 2015, Proc. Sci., Fast Transients at Cosmological Distances with the SKA. SISSA, Trieste, PoS#55
- Magrini L., Gonçalves D. R., 2009, *MNRAS*, 398, 280
- Mao S. et al., 2017, *Nat. Astron.*, 1, 621
- Marcote B., Paragi Z., 2019, preprint ([arXiv:1901.08541](https://arxiv.org/abs/1901.08541))
- Margalit B., Metzger B. D., Berger E., Nicholl M., Eftekhari T., Margutti R., 2018, *MNRAS*, 481, 2407
- Marrone D. P., Moran J. M., Zhao J.-H., Rao R., 2006, *ApJ*, 654, L57
- Masui K. et al., 2015, *Nature*, 528, 523
- McQuinn M., 2013, *ApJ*, 780, L33
- Metzger B. D., Berger E., Margalit B., 2017, *ApJ*, 841, 14
- Metzger B. D., Margalit B., Sironi L., 2019, *MNRAS*, 485, 4091
- Michilli D. et al., 2018, *Nature*, 553, 182
- Nan R. et al., 2011, *Int. J. Mod. Phys. D*, 20, 989
- Neronov A., Vovk I., 2010, *Science*, 328, 73
- Niino Y., 2018, *ApJ*, 858, 4
- Oppermann N. et al., 2015, *A&A*, 575, A118
- Pakmor R., Marinacci F., Springel V., 2014, *ApJ*, 783, L20
- Palaniswamy D., Li Y., Zhang B., 2018, *ApJ*, 854, L12
- Pen U.-L., Connor L., 2015, *ApJ*, 807, 179
- Perley D. A. et al., 2016, *ApJ*, 830, 13
- Petroff E., Hessels J. W. T., Lorimer D. R., 2019, *A&AR*, 27, 4
- Pillepich A. et al., 2019, preprint ([arXiv:1902.05553](https://arxiv.org/abs/1902.05553))
- Piro A. L., Gaensler B. M., 2018, *ApJ*, 861, 150
- Planck Collaboration I, 2014, *A&A*, 571, A1
- Platts E., Weltman A., Walters A., Tendulkar S., Gordin J., Kandhai S., *Physics Reports* (2019)
- Pol N., Lam M. T., McLaughlin M. A., Lazio T. J. W., Cordes J. M., 2019, preprint ([arXiv:1903.07630](https://arxiv.org/abs/1903.07630))
- Popov S. B., Postnov K. A., 2010, Evolution of Cosmic Objects through their Physical Activity. Proceedings of the Conference dedicated to Viktor Ambartsumian's 100th Anniversary ed HA Harutyunian, AM Mickaelian, Y. Terzian (Yerevan: NAS RA). Vol. 129. 2010. p. 129
- Prochaska J. X., Zheng Y., 2019, *MNRAS*, 485, 648
- Ravi V. et al., 2016, *Science*, 354, 1249
- Ravi V. et al., 2019, *Bull. Am. Astron. Soc.*, 51, 420
- Ravi V., Loeb A., 2018, *ApJ*, 874, 72
- Richer M. et al., 2001, *A&A*, 370, 34
- Rodrigues L. F. S., Chamandy L., Shukurov A., Baugh C. M., Taylor A. R., 2018, *MNRAS*, 483, 2424
- Salpeter E. E., 1955, *ApJ*, 121, 161
- Schober J., Schleicher D. R., Klessen R. S., 2013, *A&A*, 560, A87
- Scholz P. et al., 2016, *ApJ*, 833, 177
- Siegel M., Majewski S., Reid I., Thompson I., 2002, *ApJ*, 578, 151
- Sorce J. G. et al., 2016, *MNRAS*, 455, 2078
- Spitler L. et al., 2014, *ApJ*, 790, 101
- Spitler L. et al., 2016, *Nature*, 531, 202
- Stasyszyn F., Nuza S. E., Dolag K., Beck R., Donnert J., 2010, *MNRAS*, 408, 684
- Subramanian K., 2016, *Rep. Prog. Phys.*, 79, 076901
- Taylor A., Vovk I., Neronov A., 2011, *A&A*, 529, A144
- Tendulkar S. P. et al., 2017, *ApJ*, 834, L7
- The CHIME/FRB Collaboration, 2018, *ApJ*, 863, 48
- Trivedi P., Subramanian K., Seshadri T. R., 2014, *Phys. Rev. D*, 89, 043523
- Tully R. B. et al., 2013, *AJ*, 146, 86
- Vallée J., 1990, *AJ*, 99, 459
- Vazza F., Brüggen M., Gheller C., Hackstein S., Wittor D., Hinz P. M., 2017, *Class. Quantum Gravity*, 34, 234001
- Vazza F., Brüggen M., Hinz P. M., Wittor D., Locatelli N., Gheller C., 2018, *MNRAS*, 480, 3907
- Vergani S. et al., 2015, *A&A*, 581, A102

- Waelkens A., Jaffe T., Reinecke M., Kitaura F., Enßlin T., 2009, *A&A*, 495, 697
 Walker C. R. H., Ma Y.-Z., Breton R. P., 2018, preprint ([arXiv:1804.01548](https://arxiv.org/abs/1804.01548))
 Weisberg J. M., Cordes J. M., Kuan B., Devine K. E., Green J. T., Backer D. C., 2004, *ApJS*, 150(1), 317
 Wickramasinghe D., Ferrario L., 2008, *MNRAS*, 389, L66
 Widrow L. M., 2002, *Rev. Mod. Phys.*, 74, 775
 Wit W. d., Testi L., Palla F., Zinnecker H., 2005, *Astron. Astrophys.-Les Ulis*, 437, 247
 Woosley S., Weaver T., 1995, No. UCRL-ID-122106, Lawrence Livermore National Lab., CA (United States)
 Xu J., Han J., 2014, *MNRAS*, 442, 3329
 Xu J., Han J. L., 2015, *Res. Astron. Astrophys.*, 15, 1629
 Yang Y.-H., Zhang B.-B., Zhang B., 2019, *ApJ*, 875, L19
 Yao J., Manchester R., Wang N., 2017, *ApJ*, 835, 29
 Zhang B., 2014, *ApJ*, 780, L21
 Zhang B., 2018, *ApJ*, 867, L21
 Zheng Z., Ofek E., Kulkarni S., Neill J., Juric M., 2014, *ApJ*, 797, 71

APPENDIX A: UNIFORM PRIMORDIAL MAGNETIC FIELD

In this section, we briefly investigate the effects of choosing a uniform primordial magnetic field on the resulting RM likelihood functions. To this end, we compare the six models presented by Hackstein et al. (2018). In this paper, we used their *primordial* model, which starts with a uniform magnetic field. The other *primordial* models start from a purely turbulent field using different power-law indices, while the *astrophysical* models use a very faint seed field and instead allow for magnetic feedback from an AGN.

Using the uniform resolution grid at $z = 0$, we calculate RM for LoS parallel to two axes, positive and negative directions, to obtain both signs for RM values. From that, we obtain likelihood function of RM for the different configuration of initial magnetic field.

The result in Fig. A1 shows that for the *primordial* model, which starts from a completely uniform magnetic field, there is a pronounced peak at around 10^{-3} rad m $^{-2}$. The other *primordial2R* and *primordial3R* models start from a stochastic field, so contributions along the LoS can cancel out each other, and the likelihood reduces at the peak value and increases at lower values. Higher values, contributed by denser structures, are not affected by the shape of the primordial field. However, this feature is visible in the IGM component at order $\text{RM}_{\text{IGM}} \approx 10^{-4}$ rad m $^{-2}$, and hence not accessible. This implies that RM of FRBs do not carry information on the coherence length of primordial fields.

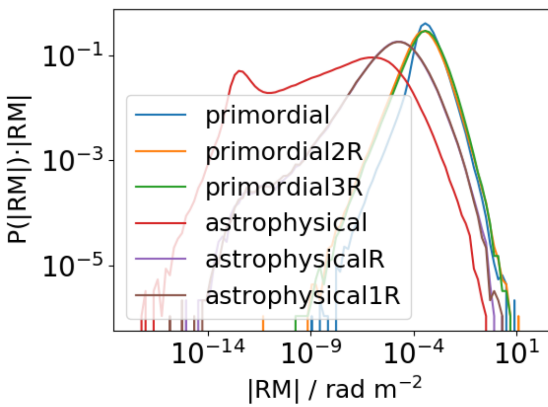


Figure A1. Likelihood function $P(\text{RM})$ for the different models of the local Universe from Hackstein et al. (2018).

The *astrophysical* models show similar highest values of RM_{IGM} to the *primordial* ones. The bulk of values is a few orders of magnitude below the *primordial* peak and the low tail reaches to substantially smaller values. The shape at low values is rather different from the results in Fig. 8 at redshift $z = 1$, as it reaches to smaller values and peaks again at around 10^{-13} rad m $^{-2}$. The difference is because predictions in this work have been reconstructed from the *primordial* model. However, since the difference in results is for values of RM that are far too low to be measurable, we consider the data sufficient for the argument of this work.

APPENDIX B: PRIORS

We perform Monte Carlo simulations in order to obtain likelihood functions for the contribution of the progenitor and the host galaxy. This requires a choice of reasonable prior probability distribution of the parameters that enter the equations. All parameters and their priors are summarized in Table B1.

We assume the source of FRBs to be magnetars, which stem from B- and O-type stars with masses of $m = 20\text{--}45 \text{ M}_\odot$ and $B_\star = 800\text{--}1500 \text{ G}$ dipole magnetic fields. This assumption is reasonable, according to the results of Wickramasinghe & Ferrario (2008). The DM and RM contribution for this case of the local environment is given by Piro & Gaensler (2018).

Woosley & Weaver (1995) showed that such supernovae explode with a typical energy of $E = 1.2 \times 10^{51}$ erg, which we adopt as a constant value.

The mass of neutron stars is about $M_{\text{NS}} \approx 1.5 \text{ M}_\odot$, regardless of the progenitor stars mass. Hence, the mass of supernova ejecta is the mass of the progenitor star m minus the mass of the neutron star. The prior of the mass of the progenitor star is given by the initial mass function, well approximated by the Salpeter function $\pi(M) \propto M^{-2.35}$ (Salpeter 1955; Chabrier 2003, 2005), and has a support in the mass range stated above, reduced by the mass of the neutron star.

We obtain the stellar radius from the radius–mass relation of heavy stars given in Derman, Demircan & Kahraman (1990).

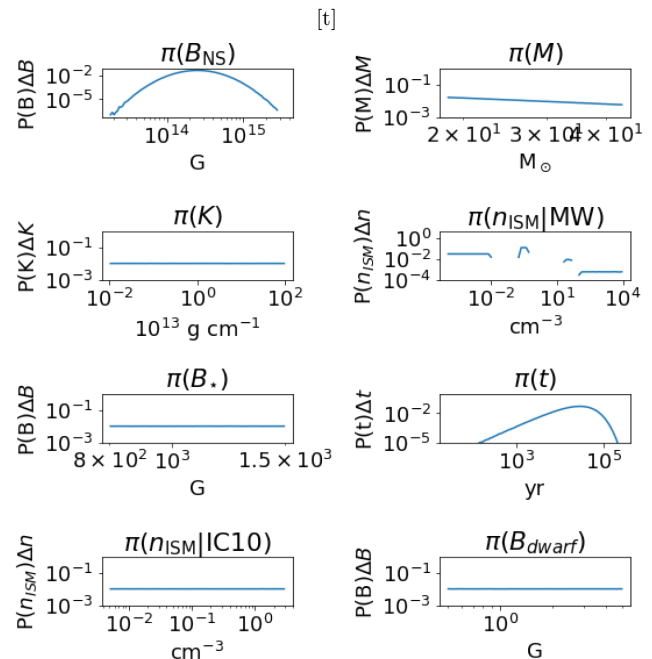


Figure B1. Graphical depiction of the priors in the Table B1.

Table B1. Parameters for Monte Carlo simulations, and their prior distributions together with a reference.**Priors:****Host galaxy**

Position of progenitor pos	$MW: \prod_{i \in [\text{thin, thick}]} e^{-\frac{z_i}{Z_i}} e^{-\frac{r_i}{R_i}}$	Siegel et al. (2002); Jurić et al. (2008)
–	$IC10: e^{-\frac{z}{Z}} e^{-\frac{r}{R}}$	Leroy et al. (2006)
Magnetic field of host B_{host}	IC10: log-flat, $B_{\text{host}} \in [0.5, 5] \mu\text{G}$	Chyžý et al. (2016)

Progenitor

Magnetic field of magnetar B_{NS}	LogNorm ($\log(2.5 \times 10^{14} \text{ G})$, 0.5)	Wickramasinghe & Ferrario (2008)
Mass of SN ejecta M	$M = m^{-2.35} - M_{\text{NS}}, m \in [20, 45] \text{ M}_{\odot}$	Chabrier (2003)
ISM number density n_{ISM}	$MW: \sum \frac{p_i}{\Delta n} (\Theta(n - n_i) - \Theta(n_{i+1} - n))$	Ferrière (2001)
–	IC10: log-flat, $n_{\text{ISM}} \in [5 \times 10^{-3}, 3]$	de Avillez & Breitschwerdt (2005)
Time since SN t	Flat, $t \in \{25 \text{ yr}, t_{\text{diss}}\}$	Margalit et al. (2018); Beloborodov & Li (2016)
Wind mass-loading parameter K	Log-flat, $K \in \{10^{11}, 10^{15}\} \text{ g cm}^{-1}$	–
Magnetic field of seed star B_{\star}	Log-flat, $B_{\star} \in \{800, 1500\} \text{ G}$	Wickramasinghe & Ferrario (2008)

The number density of the ISM, n_{ISM} , in an MW-like galaxy is highly varied across the different media found throughout the galaxy. We use the ranges of n_{ISM} given by Ferrière (2001) together with the well-known volume filling factors of the different media. Within each of these ranges, we choose a log-flat distribution, renormalized, such that the integral over the range gives the volume filling factor of the corresponding medium.

For IC10, we assume a constant n_{ISM} throughout the disc of the dwarf galaxy that falls exponentially with scale height. Since FRBs are mostly located in the disc, we use identical priors for the progenitor and the host galaxy.

In general, the production of FRBs is not related to the supernova that gives birth to the magnetar. Hence, no age of the magnetar is preferred over another, which is reflected by a flat prior. Free-free absorption by supernova ejecta can weaken FRB radiation. This implies a lower limit of $t \gtrsim 25$ yr on the age of magnetars to emit visible FRBs (Margalit et al. 2018). We adopt this value as a strict lower limit. The activity period of magnetars is limited by the dissipation of their strong magnetic field, 10^{14} – 10^{16} G. The dissipation time-scale was derived by Beloborodov & Li (2016):

$$t_{\text{diss}} = 600 \left(\frac{L}{1 \text{ km}} \right)^{1.6} \left(\frac{\delta B_{\text{NS}}}{10^{16} \text{ G}} \right)^{0.4} \left(\frac{B_{\text{NS}}}{10^{16} \text{ G}} \right)^{-1.6} \left(\frac{\rho}{\rho_{\text{nuc}}} \right)^{1.2} \text{ yr}, \quad (\text{B1})$$

where L is the typical scale of variation, δB_{NS} , of the magnetar's magnetic field strength, B_{NS} . ρ is the density of the magnetar and $\rho_{\text{nuc}} = 2.8 \times 10^{14} \text{ g cm}^{-3}$ is the nuclear saturation density. While the magnetic field dissipates, FRBs become less likely. We account for that by sampling possible values of t_{diss} and use the shape above the maximum of the resulting probability density function.

The dissipation time, t_{diss} , depends on parameters that are independent of all other parameters of interest. To sample t_{diss} , we assume typical values of $L = 10^5$ cm and $\rho = 10^{14} \text{ g cm}^{-3}$ (Beloborodov & Li 2016). For the magnetic field of the magnetar, B_{NS} , we roughly fit the results of Wickramasinghe & Ferrario (2008) with a LogNorm function centred at 2.5×10^{14} G.

The wind mass-loading parameter, K (Piro & Gaensler 2018), is not well constrained so far. Hence, we choose a log-flat prior in the expected range $K = 10^{11}$ – $10^{15} \text{ g cm}^{-1}$.

The distribution of strong magnetic fields in B- and O-type stars, B_{\star} , is rather uncertain, as is the relation between the magnetic field

of the progenitor star and that of the magnetar. This is because the strong field of the magnetar could stem from either a fossil field or a shear-driven dynamo. As a conservative choice, we use a log-flat prior for B_{\star} and consider B_{\star} and the magnetic field of the magnetar, B_{NS} , as independent.

By definition, $B_{\text{NS}} = 10^{14}$ – 10^{16} G. Wickramasinghe & Ferrario (2008) give the distribution of B_{NS} for observed magnetars and their best-fitting model. In order to minimize selection effects from observations, we adopt their best-fitting model as a LogNorm with a mean $\mu = 2.5 \times 10^{14}$ G and a logarithmic deviation $\sigma = 0.5$.

For simplicity, we assume that $\delta B_{\text{NS}} \sim B_{\text{NS}}$, which is generally the case for magnetic fields of such strength (see e.g. Beloborodov & Li 2016).

For the host galaxy, we investigate two different models: an MW-like spiral galaxy and a dwarf galaxy similar to IC10.

We assume that the probability for the position of an FRB scales with the number density of stars. In the MW-like galaxy, the best-fitting model is the combination of two discs, thin and thick, with exponential decay from centre towards the borders. We use the best-fitting parameters for the MW, given in Jurić et al. (2008), $Z_{\text{thin}} = 0.3 \text{ kpc}$, $R_{\text{thin}} = 2.6 \text{ kpc}$, $Z_{\text{thick}} = 0.9 \text{ kpc}$, and $R_{\text{thick}} = 3.6 \text{ kpc}$.

The distribution of stars in dwarf galaxies like IC10 is irregular. We hence use a simple disc model with a scale height $Z = 300 \text{ kpc}$ (Leroy et al. 2006) and a radius $R = 900 \text{ kpc}$.

de Avillez & Breitschwerdt (2005) provide a distribution of ISM density, n_{ISM} , in star-forming galaxies that is well described by a log-flat distribution and can be used as prior distribution of n_{ISM} in dwarf galaxies like IC10.

Chyžý et al. (2016) give a range of possible strengths for the ordered magnetic field of the dwarf galaxy IC10. We do not assume a particular shape, as the number of values is too low to derive a reasonable distribution. Hence, we use a log-flat distribution that covers the range of these values.

At this point, we take all our models as candidates with equal prior likelihood. The ratio of their inferred posteriors is hence equal to the ratio of their measure likelihoods, i.e. the Bayes factor.